Giant Planets

Tristan Guillot, Daniel Gautier

HAL Id: hal-00439598

https://hal.archives-ouvertes.fr/hal-00439598

Submitted on 8 Dec 2009

Giant Planets

Tristan Guillot
Observatoire de la Côte d'Azur
Laboratoire Cassiopée, CNRS UMR 6202
BP 4229
06304 Nice Cedex 4
France
guillot@obs-nice.fr

Daniel Gautier
Observatoire de Paris LESIA, CNRS FRE 2461
5 pl. J. Janssen
92195 Meudon Cedex
France
gautier@obspm.fr

Contents

The Giant Planets

Tristan Guillot
Observatoire de la Côte d'Azur

Daniel Gautier
Observatoire de Paris

Abstract

We review the interior structure and evolution of Jupiter, Saturn, Uranus and Neptune, and extrasolar giant planets with particular emphasis on constraining their global composition.

KEYWORDS: Giant planets, extrasolar planets, Jupiter, Saturn, Uranus, Neptune, planet formation

1   Introduction

In our Solar System, four planets stand out for their sheer mass and size. Jupiter, Saturn, Uranus and Neptune indeed qualify as "giant planets" because they are larger than any terrestrial planet and much more massive than all other objects in the Solar System, except the Sun, put together (fig. 1). Because of their gravitational might, they have played a key role in the formation of the Solar System, tossing around many objects in the system, preventing the formation of a planet in what is now the asteroid belt, and directly leading to the formation of the Kuiper belt and Oort cloud. They also retain some of the gas (in particular hydrogen and helium) that was present when the Sun and its planets formed and are thus key witnesses in the search for our origins.

Because of a massive envelope mostly made of hydrogen helium, these planets are *fluid*, with no solid or liquid surface. In terms of structure and composition, they lie in between stars (gaseous and mostly made of hydrogen and helium) and smaller terrestrial planets (solid and liquid and mostly made of heavy elements), with Jupiter and Saturn being closer to the former and Uranus and Neptune to the latter.

The discovery of many extrasolar planets of masses from a few hundreds down to a few Earth masses and the possibility to characterize them by the measurement of their mass and size prompts a more general definition of giant planets. For this review, we will adopt the following: "a giant planet is a planet mostly made of hydrogen and helium and too light to ignite deuterium fusion". This is purposely relatively vague – depending on whether the inventory is performed by mass or by atom or molecule, Uranus and Neptune may be included or left out of the category –. Note that Uranus and Neptune are indeed relatively different in structure than Jupiter and Saturn and are generally referred to as "ice giants", due to an interior structure that is consistent with the presence of mostly "ices" (a mixture formed from the condensation in the protoplanetary disk of low refractivity materials such as H_2O, CH_4 and NH_3, and brought to the high pressure conditions of planetary interiors –see below).
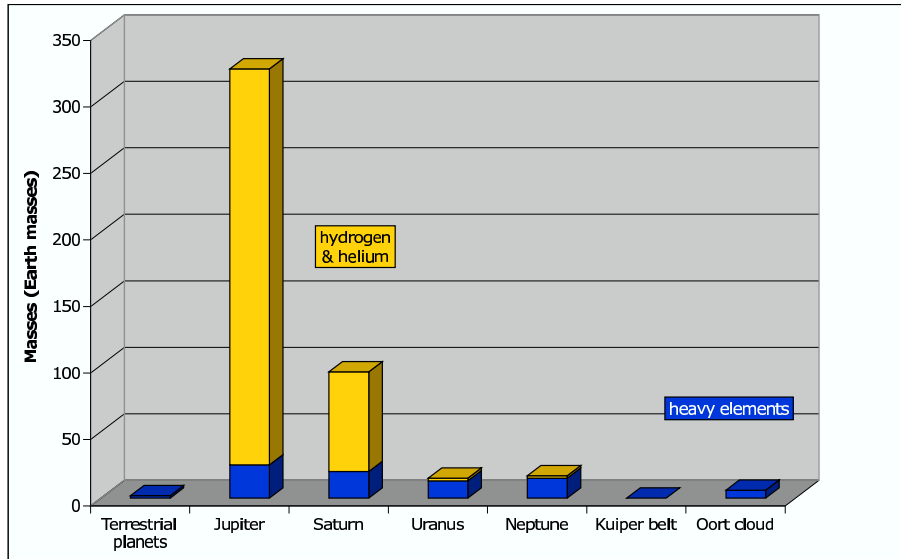
Figure 1: An inventory of hydrogen and helium and all other elements ("heavy elements") in the Solar System excluding the Sun (the Sun has a total mass of $332,960\,\mathrm{M_\oplus}$, including about $5000\,\mathrm{M_\oplus}$ in heavy elements, $1\,\mathrm{M_\oplus}$ being the mass of the Earth). The precise amount of heavy elements in Jupiter ($10-40\,\mathrm{M_\oplus}$) and Saturn ($20-30\,\mathrm{M_\oplus}$) is uncertain (see § 4.1).

Globally, this definition encompasses a class of objects that have similar properties (in particular, a low viscosity and a non-negligible compressibility) and inherited part of their material directly from the same reservoir as their parent star. These objects can thus be largely studied with the same tools, and their formation is linked to that of their parent star and the fate of the circumstellar gaseous disk present around the young star.

We will hereafter present some of the key data concerning giant planets in the Solar System and outside. We will then present the theoretical basis for the study of their structure and evolution. On this basis, the constraints on their composition will be discussed and analyzed in terms of consequences for the models of planet formation.

2 Observations and global properties

2.1 Visual appearances

In spite of its smallness, the sample of four giant planets in our Solar System exhibits a large variety of appearances, shapes, colors, variability...etc. As shown by fig. 2, all four giant planets are flattened by rotation and exhibit a more or less clear zonal wind pattern, but the color of their visible atmosphere is very different (this is due mostly to minor species in the high planetary atmosphere), their clouds have different compositions (ammonia for Jupiter and Saturn, methane for Uranus and Neptune) and depths, and their global meteorology (number of vortexes, long-lived anticyclones such as Jupiter's Great Red Spot, presence of planetary-scale storms, convective activity) is different from one planet to the next.

We can presently only wonder about what is in store for us with extrasolar giant planets since

Figure 2: Photographs of Jupiter, Saturn, Uranus and Neptune.

we cannot image them. But with orbital distances that can be as close as 0.02 AU, a variety of masses, sizes, and parent stars, we should expect to be surprised!

2.2 Gravity fields

The mass of our giant planets can be obtained with great accuracy from the observation of the motions of their natural satellites: 317.834, 95.161, 14.538 and 17.148 times the mass of the Earth ($1\,\mathrm{M}_\oplus = 5.97369 \times 10^{27}\,\mathrm{g}$) for Jupiter, Saturn, Uranus and Neptune, respectively. More precise measurements of their gravity field can be obtained through the analysis of the trajectories of spacecrafts during flyby, especially when they come close to the planet and preferably in a near-polar orbit. The gravitational field thus measured departs from a purely spherical function due to the planets' rapid rotation. The measurements are generally expressed by expanding the components of the gravity field on Legendre polynomials P_i of progressively higher orders:

$$V_{\mathrm{ext}}(r, \theta) = -\frac{GM}{r} \left\{ 1 - \sum_{i=1}^{\infty} \left(\frac{R_{\mathrm{eq}}}{r} \right)^i J_i P_i(\cos \theta) \right\}, \tag{1}$$

where $V_{\mathrm{ext}}(r, \theta)$ is the gravity field evaluated outside the planet at a distance r and colatitude θ, R_{eq} is the equatorial radius, and J_i are the gravitational moments. Because the giant planets are very close to hydrostatic equilibrium the coefficients of even order are the only ones that are not negligible. We will see how these gravitational moments, as listed in table 1, help us constrain the planets' interior density profiles.

Table 1 also indicates the radii obtained with the greatest accuracy by radio-occultation experiments. An important consequence obtained is the fact that these planets have low densities, from $0.688\,\mathrm{g\,cm}^{-3}$ for Saturn to $1.64\,\mathrm{g\,cm}^{-3}$ for Neptune, to be compared with densities of 3.9 to $5.5\,\mathrm{g\,cm}^{-3}$ for the terrestrial planets. Considering the compression that strongly increases with mass, one is led naturally to the conclusion that these planets contain an important proportion of light materials including hydrogen and helium. It also implies that Uranus and Neptune which are less massive must contain a relatively larger proportion of heavy elements than Jupiter and Saturn. This may lead to a sub-classification between the hydrogen-helium giant planets Jupiter and Saturn, and the "ice giants" or "sub giants" Uranus and Neptune.

The planets are also relatively fast rotators, with periods of ~ 10 hours for Jupiter and Saturn, and ~ 17 hours for Uranus and Neptune. The fact that this fast rotation visibly affects the figure (shape) of these planets is seen by the significant difference between the polar and equatorial radii. It also leads to gravitational moments that differ significantly from a nul value. However, it is

Table 1: Characteristics of the gravity fields and radii

	Jupiter	Saturn	Uranus	Neptune
$M \times 10^{-26}$ [kg]	18.986112(15)[a]	5.684640(30)[b]	0.8683205(34)[c]	1.0243542(31)[d]
$R_{\rm eq} \times 10^{-7}$ [m]	7.1492(4)[e]	6.0268(4)[f]	2.5559(4)[g]	2.4766(15)[g]
$R_{\rm pol} \times 10^{-7}$ [m]	6.6854(10)[e]	5.4364(10)[f]	2.4973(20)[g]	2.4342(30)[g]
$\overline{R} \times 10^{-7}$ [m]	6.9894(6)[h]	5.8210(6)[h]	2.5364(10)[i]	2.4625(20)[i]
$\overline{\rho} \times 10^{-3}$ [kg m^{-3}]	1.3275(4)	0.6880(2)	1.2704(15)	1.6377(40)
$J_2 \times 10^2$	1.4697(1)[a]	1.632425(27)[b]	0.35160(32)[c]	0.3539(10)[d]
$J_4 \times 10^4$	$-5.84(5)$[a]	$-9.397(28)$[b]	$-0.354(41)$[c]	$-0.28(22)$[d]
$J_6 \times 10^4$	0.31(20)[a]	0.867(97)[b]	...	...
$P_\omega \times 10^{-4}$ [s]	3.57297(41)[j]	3.83624(47) ?[j,k]	6.206(4)[l]	5.800(20)[m]
q	0.08923(5)	0.15491(10)	0.02951(5)	0.02609(23)
$C/MR_{\rm eq}^2$	0.258	0.220	0.230	0.241

The numbers in parentheses are the uncertainty in the last digits of the given value. The value of the gravitational constant used to calculate the masses of Jupiter and Saturn is $G = 6.67259 \times 10^{-11}$ N m^2 kg^{-2} (Cohen and Taylor, 1987). The values of the radii, density and gravitational moments correspond to the one bar pressure level (1 bar= 10^5 Pa).
[a] Campbell and Synnott (1985)
[b] Jacobson et al. (2006)
[c] Anderson et al. (1987)
[d] Tyler et al. (1989)
[e] Lindal et al. (1981)
[f] Lindal et al. (1985)
[g] Lindal (1992a)
[h] From 4th order figure theory
[i] $(2R_{\rm eq} + R_{\rm pol})/3$ (Clairaut's approximation)
[j] Davies et al. (1986)
[k] This measurement from the *Voyager* era is now in question and values up to 38826 s have been proposed (see § 2.3)
[l] Warwick et al. (1986)
[m] Warwick et al. (1989)

important to stress that there is no unique rotation frame for these fluid planets: atmospheric zonal winds imply that different latitude rotate at different velocities (see § 2.6), and the magnetic field provides an other rotation period. Because the latter is tied to the deeper levels of the planet, it is believed to be more relevant when interpreting the gravitational moments. The rotation periods listed in Table 1 hence correspond to that of the magnetic field. The case of Saturn appears to be complex and is discussed in the next section.

2.3   Magnetic fields

As the Earth, the Sun and Mercury, our four giant planets possess their own magnetic fields, as shown by the Voyager 2 measurements. The structures of these magnetic fields are very different from one planet to another and the dynamo mechanism that generates them is believed to be related to convection in their interior but is otherwise essentially unknown (see Stevenson, 1983, for a review).

The magnetic field **B** is generally expressed in form of a development in spherical harmonics of

the scalar potential W, such that $\mathbf{B} = -\boldsymbol{\nabla} W$:

$$W = a \sum_{n=1}^{\infty} \left(\frac{a}{r}\right)^{n+1} \sum_{m=0}^{n} \left\{g_n^m \cos(m\phi) + h_n^m \sin(m\phi)\right\} P_n^m(\cos\theta). \qquad (2)$$

r is the distance to the planet's center, a its radius, θ the colatitude, ϕ the longitude and P_n^m the associated Legendre polynomials. The coefficients g_n^m and h_n^m are the magnetic moments that characterize the field. They are expressed in magnetic field units.

One can show that the first coefficients of relation (2) (for $n = 0$ and $n = 1$) correspond to the potential of a magnetic dipole such that $W = \mathbf{M} \cdot \mathbf{r}/r^3$ of moment:

$$M = a^3 \left\{ \left(g_1^0\right)^2 + \left(g_1^1\right)^2 + \left(h_1^1\right)^2 \right\}^{1/2}. \qquad (3)$$

Jupiter and Saturn have magnetic fields of essentially dipolar nature, of axis close to the rotation axis (g_1^0 is much larger than the other harmonics); Uranus and Neptune have magnetic fields that are intrinsically much more complex. To provide an idea of the intensity of the magnetic fields, the value of the dipolar moments for the four planets are 4.27 Gauss R_J^3, 0.21 Gauss R_S^3, 0.23 Gauss R_U^3, 0.133 Gauss R_N^3, respectively (Connerney et al., 1982; Acuna et al., 1983; Ness et al., 1986, 1989).

A true surprise from *Voyager* that has been confirmed by the *Cassini-Huygens* mission is that Saturn's magnetic field is axisymmetric *to the limit of the measurement accuracy*: Saturn's magnetic and rotation axes are perfectly aligned. Voyager measurements indicated nevertheless a clear signature in the radio signal at 10h 39min 22s believed to be a consequence of the rotation of the magnetic field. Determinations of a magnetic anomaly and new measurements by Cassini have since considerably blurred the picture, and the interpretation of the measurements have become unclear, with a deep rotation period evaluated between that of Voyager and as slow as 10h 47min 6s (Gurnett et al., 2005; Giampieri et al., 2006) (see also Galopeau and Lecacheux, 2000; Cecconi and Zarka, 2005). Note that models discussed hereafter have not yet included this additional uncertainty.

2.4 Atmospheric compositions

In fluid planets, the distinction between the atmosphere and the interior is not obvious. We name "atmosphere" the part of the planet which can directly exchange radiation with the exterior environment. This is also the part which is accessible by remote sensing. It is important to note that the continuity between the atmosphere and the interior does not guarantee that compositions measured in the atmosphere can be extrapolated to the deep interior, even in a fully convective environment: Processes such as phase separations (e.g. Salpeter, 1973; Stevenson and Salpeter, 1977b; Fortney and Hubbard, 2003), phase transitions (e.g. Hubbard, 1989), chemical reactions (e.g. Fegley and Lodders, 1994) can occur and decouple the surface and interior compositions. Furthermore, imperfect mixing may also occur, depending on the initial conditions (e.g. Stevenson, 1985).

The conventional wisdom is however that these processes are limited to certain species (e.g. helium) or that they have a relatively small impact on the global abundances, so that the hydrogen-helium envelopes may be considered relatively uniform, from the perspective of the global abundance in heavy elements. We first discuss measurements made in the atmosphere before inferring interior compositions from interior and evolution models.

2.4.1 Hydrogen and helium

The most important components of the atmospheres of our giant planets are also among the most difficult to detect: H_2 and He have a zero dipolar moment and hence absorb very inefficiently visible and infrared light. Their infrared absorption becomes important only at high pressures when collision-induced absorption becomes significant (e.g. Borysow et al., 1997). On the other hand, lines due to electronic transitions correspond to very high altitudes in the atmosphere, and bear little information on the structure of the deeper levels. The only robust result concerning the abundance of helium in a giant planet is by *in situ* measurement by the Galileo probe in the atmosphere of Jupiter (von Zahn et al., 1998). The helium mole fraction (*i.e.* number of helium atoms over the total number of species in a given volume) is $q_{\text{He}} = 0.1359 \pm 0.0027$. The helium mass mixing ratio Y (*i.e.* mass of helium atoms over total mass) is constrained by its ratio over hydrogen, X: $Y/(X+Y) = 0.238 \pm 0.05$. This ratio is by coincidence that found in the Sun's atmosphere, but because of helium sedimentation in the Sun's radiative zone, it was larger in the protosolar nebula: $Y_{\text{proto}} = 0.275 \pm 0.01$ and $(X+Y)_{\text{proto}} \approx 0.98$ (e.g. Bahcall et al., 1995). Less helium is therefore found in the atmosphere of Jupiter than inferred to be present when the planet formed. We will discuss the consequences of this measurement later: let us mention that the explanation invokes helium settling due to a phase separation in the interiors of massive and cold giant planets.

Helium is also found to be depleted compared to the protosolar value in Saturn's atmosphere. However, in this case the analysis is complicated by the fact that Voyager radio occultations apparently led to a wrong value. The current adopted value is now $Y = 0.18 - 0.25$ (Conrath and Gautier, 2000), in agreement with values predicted by interior and evolution models (Guillot, 1999b; Hubbard et al., 1999). Finally, Uranus and Neptune are found to have near-protosolar helium mixing ratios, but with considerable uncertainty.

2.4.2 Heavy elements

The abundance of other elements than hydrogen and helium (that we will call hereafter "heavy elements") bears crucial information for the understanding of the processes that led to the formation of these planets.

The most abundant heavy elements in the envelopes of our four giant planets are O, C, N, S. It is possible to model the chemistry of gases in the tropospheres from the top of the convective zone down to the 2000 K temperature level (Fegley and Lodders, 1994). Models conclude that, whatever the initial composition in these elements of planetesimals which collapsed with hydrogen onto Jupiter and Saturn cores during the last phase of the planetary formation, C in the upper tropospheres of giant planets is mainly in the form of gaseous CH_4, N in the form of NH_3, S in the form of H_2S, and O in the form of H_2O. All these gases, but methane in Jupiter and Saturn, condense in the upper troposphere, but vaporize at deeper levels when the temperature increases. Interestingly enough, noble gases are not expected to condense even at the cold tropopause temperatures of Uranus and Neptune.

The mass spectrometer aboard the Galileo atmospheric probe has performed in situ measurements of Ar, Kr, Xe, CH_4, NH_3, H_2S, and H_2O in the troposphere of Jupiter. C, N, and S were found to be oversolar by a factor 3 to 4 (Wong et al., 2004), which was not unexpected because condensation of nebula gases results in enriching icy grains and planetesimals. The surprise came from Ar, Kr, Xe, which were expected to be solar because they are difficult to condense, but turned out to be oversolar by factors 2 to 4 (Owen et al., 1999; Wong et al., 2004). One exception among these enriched species was neon, which was found to be significantly undersolar, but was

Table 2: Main gaseous components of heavy elements measured in the troposphere of giant planets

	Species	Mixing ratio/H_2	References	Comments
Jupiter	CH_4	$(2.37 \pm 0.37) \times 10^{-3}$	Wong et al. (2004)	GPMS on Galileo(1)
	NH_3	$(6.64 \pm 2.34) \times 10^{-3}$	Wong et al. (2004)	*idem*
	H_2S	$(8.9 \pm 2.1) \times 10^{-3}$	Wong et al. (2004)	*idem*
	H_2O	$(4.9 \pm 1.6) \times 10^{-4}$	Wong et al. (2004)	*idem*; region not well mixed
	^{36}Ar	$(6.1 \pm 1.2) \times 10^{-6}$	Atreya et al. (1999)	*idem*
	^{84}Kr	$(1.84 \pm 0.37) \times 10^{-9}$	Atreya et al. (1999)	*idem*
	^{132}Xe	$(4.9 \pm 1.0) \times 10^{-11}$	Atreya et al. (1999)	*idem*
Saturn	CH_4	$(4.3 \pm 1) \times 10^{-3}$	Flasar et al. (2005)	CIRS on Cassini (3)
	NH_3	$(1 \pm 1) \times 10^{-4}$	Briggs and Sackett (1989)	Ground-based microwave (4)
	H_2S	$(2.2 \pm 0.3) \times 10^{-4}$	Briggs and Sackett (1989)	*idem*
Uranus	CH_4	$(3.3 \pm 1.1) \times 10^{-2}$	Gautier et al. (1995)	Compilation from ground-based observations
	H_2S	$(1 \pm 1) \times 10^{-4}$	Briggs and Sackett (1989)	Ground-based microwave (4)
Neptune	CH_4	$(3.3 \pm 1.1) \times 10^{-2}$	Gautier et al. (1995)	Compilation from ground-based observations
	H_2S	$(7.5 \pm 3.25) \times 10^{-4}$	de Pater et al. (1991)	Ground based microwave (5)
	H_2O	$7.7 \times 10(-1)$	Lodders and Fegley (1994)	Inferred from CO (6)

(1) Galileo Probe Mass Spectrometer aboard the atmospheric probe in Jupiter

(2) The signal stopped at the 22 bar levels prior to have reached a constant value. It is currently believed that the region where the probe made measurementds was atypically dry and that the bulk abundance of H_2O in Jupiter has not been measured.

(3) Composite Infra Red Spectrometer aboard the Cassini spacecraft

(4) Ground based measurements of the microwave continuum. The result is somewhat uncertain due to the difficulty to precisely estimate opacities of absorbing species

(5) Ground based microwave measurements. An oversolar H_2S abundance is required to interpret the depletion of NH_3 in the upper troposphere

(6) Inferred from the microwave detection of CO in the troposphere. Note that the validity of the approach is questionned by Bézard et al. (2002). A large amount of water seems to be present anyway in the deep atmosphere of Neptune. The case of Uranus is still uncertain because it is not known so far if CO is present in the troposphere of the planet.

predicted to be so because of a capture by the falling helium droplets (Roulston and Stevenson, 1995). Another exception was water, but this molecule is affected by meteorological processes, and the probe was shown to have fallen into a dry region of Jupiter's atmosphere.

Specifically, CH_4/H_2 has been found oversolar in the four giant planets: the C/H ratio corresponding to the measured abundances is always higher than the solar C/H ratio, and in fact appears to be increasing with distance to the Sun. C/H is 3, 7.5, 45 and 45 times solar, in Jupiter, Saturn, Uranus and Neptune, respectively. Note that the quoted enrichments are subject to changes when the solar abundances tables are revised, which happens surprisingly frequently.

Except for Jupiter, the determination of the NH_3 abundance is more uncertain than that of CH_4 because it is model dependant. It is derived from fitting microwave spectra of giant planets which exhibit a continuum opacity, more difficult to model than absorption spectral lines. However, the N/H enrichment seems to be, so far, fairly constant from a planet to another, around a factor 2, so that C/N is higher in Saturn than in Jupiter, and still higher in Uranus and Neptune.

H_2S has been measured in situ in Jupiter, but in the three other giant planets its large abundance is derived from the requirement to deplete NH3 at deeper levels than the saturation one;

This scenario has been proposed a long time ago by Gulkis et al. (1978). It implies that S/H is substantially oversolar in Uranus and in Neptune.

H_2O is difficult to measure in all four giant planets because of its condensation relatively deep. It was hoped that the Galileo probe would provide a measurement of its deep abundance, but the probe fell into one of Jupiter's 5-microns hot spot, what is now believed to be a dry region mostly governed by downwelling motions (e.g. Showman and Ingersoll, 1998). As a result, and although the probe provided measurements down to 22 bars, well below water's canonical 5 bar cloud base, it is believed that this measurement of a water abundance equal to a fraction of the solar value is only a lower limit.

2.5   Energy balance and atmospheric temperature profiles

Jupiter, Saturn and Neptune are observed to emit significantly more energy than they receive from the Sun (see Table 3). The case of Uranus is less clear. Its intrinsic heat flux $F_{\rm int}$ is significantly smaller than that of the other giant planets. Detailed modeling of its atmosphere however indicate that $F_{\rm int} \gtrsim 60\,{\rm erg\,cm^{-2}\,s^{-1}}$ (Marley and McKay, 1999). With this caveat, all four giant planets can be said to emit more energy than they receive from the Sun. Hubbard (1968) showed in the case of Jupiter that this can be explained simply by the progressive contraction and cooling of the planets.

Table 3: Energy balance as determined from Voyager IRIS data[a].

	Jupiter	Saturn	Uranus	Neptune
Absorbed power [10^{16} J s^{-1}]	50.14±2.48	11.14±0.50	0.526±0.037	0.204±0.019
Emitted power [10^{16} J s^{-1}]	83.65±0.84	19.77±0.32	0.560±0.011	0.534±0.029
Intrinsic power [10^{16} J s^{-1}]	33.5±2.6	8.63±0.60	$0.034^{+0.038}_{-0.034}$	0.330±0.035
Intrinsic flux [J s^{-1} m^{-2}]	5.44±0.43	2.01±0.14	$0.042^{+0.047}_{-0.042}$	0.433±0.046
Bond albedo []	0.343±0.032	0.342±0.030	0.300±0.049	0.290±0.067
Effective temperature [K]	124.4±0.3	95.0±0.4	59.1±0.3	59.3±0.8
1-bar temperature[b] [K]	165±5	135±5	76±2	72±2

[a] After Pearl and Conrath (1991)
[b] Lindal (1992b)

A crucial consequence of the presence of an intrinsic heat flux is that it requires high internal temperatures ($\sim 10,000\,{\rm K}$ or more), and that consequently the giant planets are *fluid* (not solid) (Hubbard (1968); see also Hubbard et al. (1995)). Another consequence is that they are essentially convective, and that their interior temperature profile are close to *adiabats*. We will come back to this in more detail.

The deep atmospheres (more accurately tropospheres) of the four giant planets are indeed observed to be close to adiabats, a result first obtained by spectroscopic models (Trafton, 1967), then verified by radio-occultation experiments by the Voyager spacecrafts, and by the *in situ* measurement from the Galileo probe (fig. 3). The temperature profiles show a temperature minimum, in a region near 0.2 bar called the tropopause. At higher altitudes, in the stratosphere, the temperature gradient is negative (increasing with decreasing pressure). In the regions that we will be mostly concerned with, in the troposphere and in the deeper interior, the temperature always increases with depth. It can be noticed that the slope of the temperature profile in fig 3 becomes almost constant when the atmosphere becomes convective, at pressures of a few tens of bars, in the four
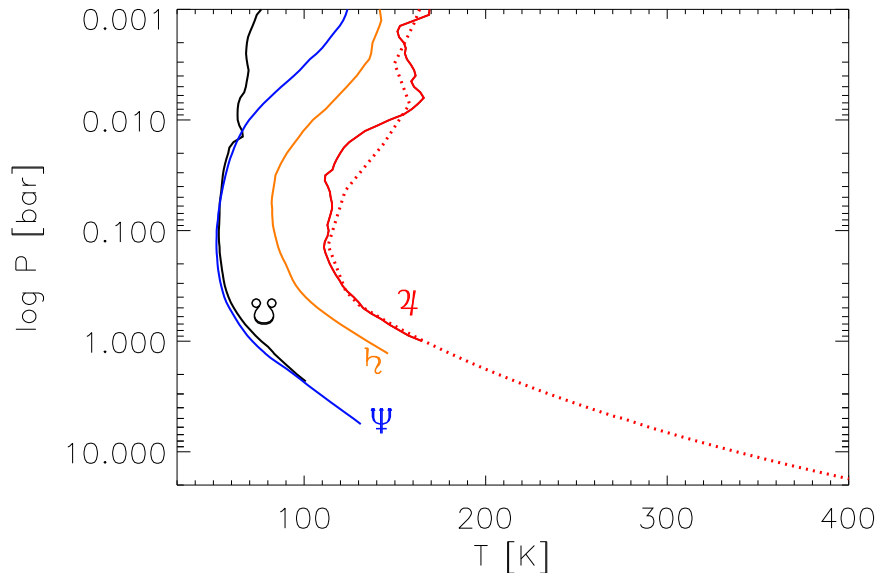
giant planets.

Figure 3: Atmospheric temperatures as a function of pressure for Jupiter, Saturn, Uranus and Neptune, as obtained from Voyager radio-occultation experiments (see Lindal, 1992b). The dotted line corresponds to the temperature profile retrieved by the Galileo probe, down to 22 bar and a temperature of 428 K (Seiff et al., 1998).

It should be noted that the 1 bar temperatures listed in table 3 and the profiles shown in Fig. 3 are retrieved from radio-occultation measurements using a helium to hydrogen ratio which, at least in the case of Jupiter and Saturn, was shown to be incorrect. The new values of Y are found to lead to increased temperatures by $\sim 5\,\mathrm{K}$ in Jupiter and $\sim 10\,\mathrm{K}$ in Saturn (see Guillot, 1999a). However, the Galileo probe found a 1 bar temperature of $166\,\mathrm{K}$ (Seiff et al., 1998), and generally a good agreement with the Voyager radio-occultation profile with the wrong He/H$_2$ value.

When studied at low spatial resolution, it is found that all four giant planets, in spite of their inhomogeneous appearances, have a rather uniform brightness temperature, with pole-to-equator latitudinal variations limited to a few kelvins (*e.g.* Ingersoll et al., 1995). However, in the case of Jupiter, some small regions are known to be very different from the average of the planet. This is the case of hot spots, which cover about 1% of the surface of the planet at any given time, but contribute to most of the emitted flux at 5 microns, due to their dryness (absence of water vapor) and their temperature brightness which can, at this wavelength, peak to $260\,\mathrm{K}$.

2.6 Atmospheric dynamics: winds and weather

The atmospheres of all giant planets are evidently complex and turbulent in nature. This can for example be seen from the mean zonal winds (inferred from cloud tracking), which are very rapidly varying functions of the latitude (see *e.g.* Ingersoll et al., 1995): while some of the regions rotate

at the same speed as the interior magnetic field (in the so-called "system III" reference frame), most of the atmospheres do not. Jupiter and Saturn both have superrotating equators (+100 and +400 m s^{-1} in system III, for Jupiter and Saturn, respectively), Uranus and Neptune have subrotating equators, and superrotating high latitude jets. Neptune, which receives the smallest amount of energy from the Sun has the largest peak-to-peak latitudinal variations in wind velocity: about 600 m s^{-1}. It can be noted that, contrary to the case of the strongly irradiated planets to be discussed later, the winds of Jupiter, Saturn, Uranus and Neptune, are significantly slower than the planet itself under its own spin (from 12.2 km s^{-1} for Jupiter to 2.6 km s^{-1} for Neptune, at the equator).

The observed surface winds are believed to be related to motions in the planets' interiors, which, according to the Taylor-Proudman theorem, should be confined by the rapid rotation to the plane perpendicular to the axis of rotation (*e.g.* Busse, 1978). Unfortunately, no convincing model is yet capable of modeling with sufficient accuracy both the interior and the surface layers.

Our giant planets also exhibit planetary-scale to small-scale storms with very different temporal variations. For example, Jupiter's great red spot is a 12000 km-diameter anticyclone found to have lasted for at least 300 years (e.g. Simon-Miller et al., 2002). Storms developing over the entire planet have even been observed on Saturn (Sanchez-Lavega et al., 1996). Uranus and Neptune's storm system has been shown to have been significantly altered since the Voyager era (Rages et al., 2002; Hammel et al., 2005). On Jupiter, small-scale storms related to cumulus-type cloud systems have been observed (e.g. Gierasch et al., 2000; Hueso et al., 2002), and lightning strikes have been monitored by Galileo (e.g. Little et al., 1999). These represent only a small arbitrary subset of the work concerning the complex atmospheres of these planets.

It is tempting to extrapolate these observations to the objects outside our Solar System as well. However, it is important to stress that an important component of the variability in the atmospheres of our giant planets is the presence of relatively abundant condensing chemical species: ammonia and water in the case of Jupiter and Saturn, and methane for Uranus and Neptune. These species can only condense in very cold atmospheres, thus providing latent heat to fuel important storms. Depending on their temperatures and compositions, extrasolar planets may or may not possess such important condensing species (e.g. Guillot, 1999b).

2.7 Moons and rings

A discussion of our giant planets motivated by the opportunity to extrapolate the results to objects outside our solar system would be incomplete without mentioning the moons and rings that these planets all possess (see chapters by Breuer & Moore, by Peale and by Husmann et al.). First, the satellites/moons can be distinguished from their orbital characteristics as regular or irregular. The first ones have generally circular, prograde orbits. The latter tend to have eccentric, extended, and/or retrograde orbits.

These satellites are numerous: After the Voyager era, Jupiter was known to possess 16 satellites, Saturn to have 18, Uranus 20 and Neptune 8. Recent extensive observation programs have seen the number of satellites increase considerably, with a growing list of satellites presently reaching 62, 56, 27 and 13 for Jupiter, Saturn, Uranus and Neptune, respectively. All of the new satellites discovered since Voyager are classified as irregular.

The presence of regular and irregular satellites is due in part to the history of planet formation. It is believed that the regular satellites have mostly been formed in the protoplanetary subnebulae that surrounded the giant planets (at least Jupiter and Saturn) at the time when they accreted their envelopes. On the other hand, the irregular satellites are thought to have been captured by

the planet. This is for example believed to be the case of Neptune's largest moon, Triton, which has a retrograde orbit.

A few satellites stand out by having relatively large masses: it is the case of Jupiter's Io, Europa, Ganymede and Callisto, of Saturn's Titan, and of Neptune's Triton. Ganymede is the most massive of them, being about twice the mass of our Moon. However, compared to the mass of the central planet, these moons and satellites have very small weights: 10^{-4} and less for Jupiter, 1/4000 for Saturn, 1/25000 for Uranus and 1/4500 for Neptune. All these satellites orbit relatively closely to their planets. The farthest one, Callisto revolves around Jupiter in about 16 Earth days.

The four giant planets also have rings, whose material is probably constantly resupplied from their satellites. The ring of Saturn stands out as the only one directly visible with binoculars. In this particular case, its enormous area allows it to reflect a sizable fraction of the stellar flux arriving at Saturn, and makes this particular ring as bright as the planet itself. The occurrence of such rings would make the detection of extrasolar planets slightly easier, but it is yet unclear how frequent they can be, and how close to the stars rings can survive both the increased radiation and tidal forces.

2.8 Extrasolar planets
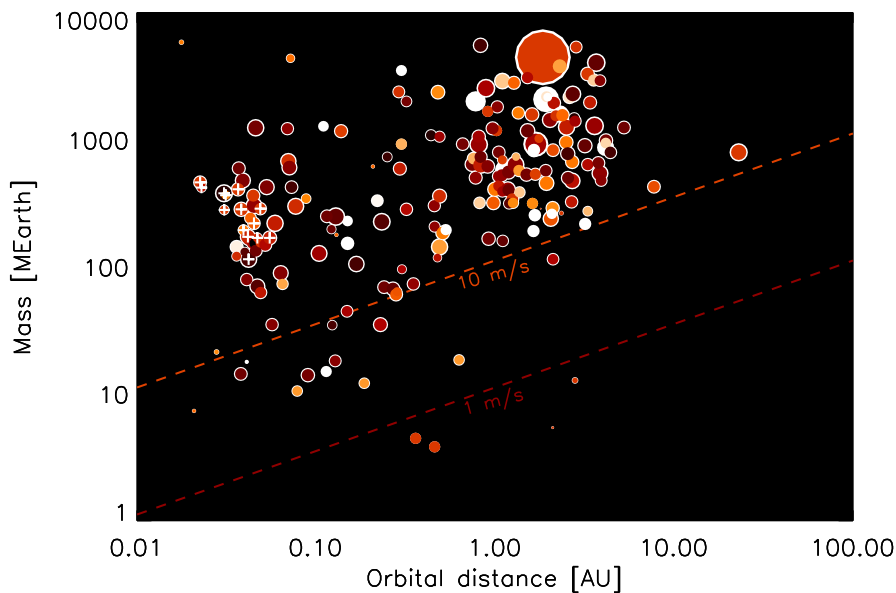
Figure 4: Masses and orbital distances of the extrasolar planets discovered by 2006. The size of the symbols is proportional to the mass of the parent star (from 0.1 to 4 stellar masses). The color (from white to red and black) is proportional to the stellar metallicity. Stars with metallicities [Fe/H] < 0.2 are shown in white. The radial velocimetry thresholds at 1 and 10 m/s, encompassing the detection limits of most current surveys, are indicated as dashed lines. *Transiting* planets are highlighted with white crosses.

Huge progresses have been made in the field of extrasolar planets since the detection of the first giant planet orbiting a solar-type star by Mayor and Queloz (1995). More than 200 planets are known at the time of this review, and importantly, 14 planets that transit their star at each orbital revolution have been identified (see fig 4). These transiting planets are especially interesting because of the possibility to measure both their mass and size and thus obtain constraints on their global composition.

In spite of their particular location just a few stellar radii away from their stars, the transiting planets that have been discovered bear some resemblance with their Solar System cousins in the sense that they are also mostly made of hydrogen and helium (e.g. Burrows et al., 2000; Guillot, 2005; Baraffe et al., 2005). They are, however, much hotter due to the intense irradiation that they receive.

Although obtaining direct informations on these planets represent a great observational challenge, several key steps have been accomplished: Atomic Sodium, predicted to be detectable (Seager and Sasselov, 2000), has indeed been detected by transit spectroscopy around one planet (Charbonneau et al., 2002). Hydrodynamically escaping hydrogen, oxygen and carbon have also been detected from the same planet (Vidal-Madjar et al., 2003, 2004). The measurement of the *secondary* eclipse of several planets by the Spitzer satellite allowed a constraint on spectral and hence thermal properties of the planetary atmospheres (Charbonneau et al., 2005; Deming et al., 2005). Recently, the light curve of a non-transiting planet was detected in the infrared, also with Spitzer, providing preliminary indications of a strong day/night temperature variation (Harrington et al., 2006) perhaps even larger than predicted (see Showman and Guillot, 2002).

Obviously, there is a big potential for growth in this young field, and the comparison between fine observations made for giant planets in our Solar System and the more crude, but also more statistically significant data obtained for planets around other stars promises to be extremely fruitful to better understand these objects.

3   The calculation of interior and evolution models

3.1   Basic equations

The structure and evolution of a giant planet is governed by the following hydrostatic, thermodynamic, mass conservation and energy conservation equations:

$$\frac{\partial P}{\partial r} = -\rho g \tag{4}$$

$$\frac{\partial T}{\partial r} = \frac{\partial P}{\partial r}\frac{T}{P}\nabla_T. \tag{5}$$

$$\frac{\partial m}{\partial r} = 4\pi r^2 \rho. \tag{6}$$

$$\frac{\partial L}{\partial r} = 4\pi r^2 \rho \left(\dot{\epsilon} - T\frac{\partial S}{\partial t}\right), \tag{7}$$

where P is the pressure, ρ the density, and $g = Gm/r^2$ the gravity (m is the mass, r the radius and G the gravitational constant). The temperature gradient $\nabla_T \equiv (d\ln T/d\ln P)$ depends on the process by which the internal heat is transported. L is the intrinsic luminosity, t the time, S the specific entropy (per unit mass), and $\dot{\epsilon}$ accounts for the sources of energy due e.g. to radioactivity or more importantly nuclear reactions. Generally it is a good approximation to assume $\dot{\epsilon} \sim 0$ for

objects less massive than $\sim 13\,M_J$, i.e. too cold to even burn deuterium (but we will see that in certain conditions this term may be useful, even for low mass planets).

The boundary condition at the center is trivial: $r = 0$; ($m = 0$, $L = 0$). The external boundary condition is more difficult to obtain because it depends on how energy is transported in the atmosphere. One possibility is to use the Eddington approximation, and to write (e.g. Chandrasekhar, 1939): $r = R$; ($T_0 = T_{\rm eff}$, $P_0 = 2/3\,g/\kappa$), where $T_{\rm eff}$ is the effective temperature (defined by $L = 4\pi R\sigma T_{\rm eff}^4$, with σ being the Stephan-Boltzmann constant), and κ is the opacity. Note for example that in the case of Jupiter $T_{\rm eff} = 124\,{\rm K}$, $g = 26\,{\rm m\,s^{-2}}$ and $\kappa \approx 5 \times 10^{-3}(P/1\,{\rm bar})\,{\rm m^2\,kg^{-1}}$. This implies $P_0 \approx 0.2\,{\rm bar}$ (20,000 Pa), which is actually close to Jupiter's tropopause, where $T \approx 110\,{\rm K}$.

More generally, one has to use an atmospheric model relating the temperature and pressure at a given level to the radius R, intrinsic luminosity L and incoming stellar luminosity $L_{*\rm p}$: $r = R$; ($T_0 = T_0(R, L, L_{*\rm p})$, $P_0 = P_0(R, L, L_{*\rm p})$). P_0 is chosen to satisfy the condition that the corresponding optical depth at that level should be much larger than unity. If the stellar flux is absorbed mostly in a convective zone, then the problem can be simplified by using $T_0(R, L, L_{*\rm p}) \approx T_0(R, L + L_{*\rm p}, 0)$ (e.g. Hubbard, 1977). An example of such a model is described by Saumon et al. (1996) and Hubbard et al. (2002) and is used hereafter to model the planets in the low irradiation limit.

3.2   High pressure physics & equations of state

In terms of pressures and temperatures, the interiors of giant planets lie in a region for which accurate equations of state (EOS) are extremely difficult to calculate. This is because both molecules, atoms, and ions can all coexist, in a fluid that is partially degenerate (free electrons have energies that are determined both by quantum and thermal effects) and partially coupled (coulomb interactions between ions are not dominant but must be taken into account). The presence of many elements and their possible interactions further complicate matters. For lack of space, this section will mostly focus on hydrogen whose EOS has seen the most important developments in recent years. A phase diagram of hydrogen (fig. 5) illustrates some of the important phenomena that occur in giant planets.

The photospheres of giant planets are generally relatively cold (50 to 3000 K) and at low pressure (0.1 to 10 bar, or 10^4 to 10^6 Pa), so that hydrogen is in molecular form and the perfect gas conditions apply. As one goes deeper into the interior hydrogen and helium progressively become fluid. (The perfect gas relation tends to underestimate the pressure by 10% or more when the density becomes larger than about $0.02\,{\rm g\,cm^{-3}}$ ($P \gtrsim 1\,{\rm kbar}$ in the case of Jupiter)).

Characteristic interior pressures are considerably larger however: as implied by Eqs. 4 and 6, $P_{\rm c} \approx GM^2/R^4$, of the order of 10-100 Mbar for Jupiter and Saturn. At these pressures and the corresponding densities, the Fermi temperature $T_{\rm F}$ is larger than 10^5 K. This implies that electrons are degenerate. Figure 5 shows that inside Jupiter, Saturn, the extrasolar planet HD 209458 b, but also for giant planets in general for most of their history, the degeneracy parameter $\theta = T/T_{\rm F}$ is between 0.1 and 0.03. Therefore, the energy of electrons in the interior is expected to be only slightly larger than their non-relativistic, fully degenerate limit: $u_{\rm e} \geq 3/5\,kT_{\rm F} = 15.6\,(\rho/\mu_{\rm e})^{2/3}$ eV, where k is Boltzmann's constant, $\mu_{\rm e}$ is the number of electrons per nucleon and ρ is the density in $\rm g\,cm^{-3}$. For pure hydrogen, when the density reaches $\sim 0.8\,{\rm g\,cm^{-3}}$, the average energy of electrons becomes larger than hydrogen's ionization potential, even at zero temperature: hydrogen pressure-ionizes and becomes metallic. This molecular to metallic transition occurs near Mbar pressures, but exactly how this happens remains unclear because of the complex interplay of thermal, coulomb, and degeneracy effects (in particular, whether hydrogen metallizes into an atomic state H^+ — as
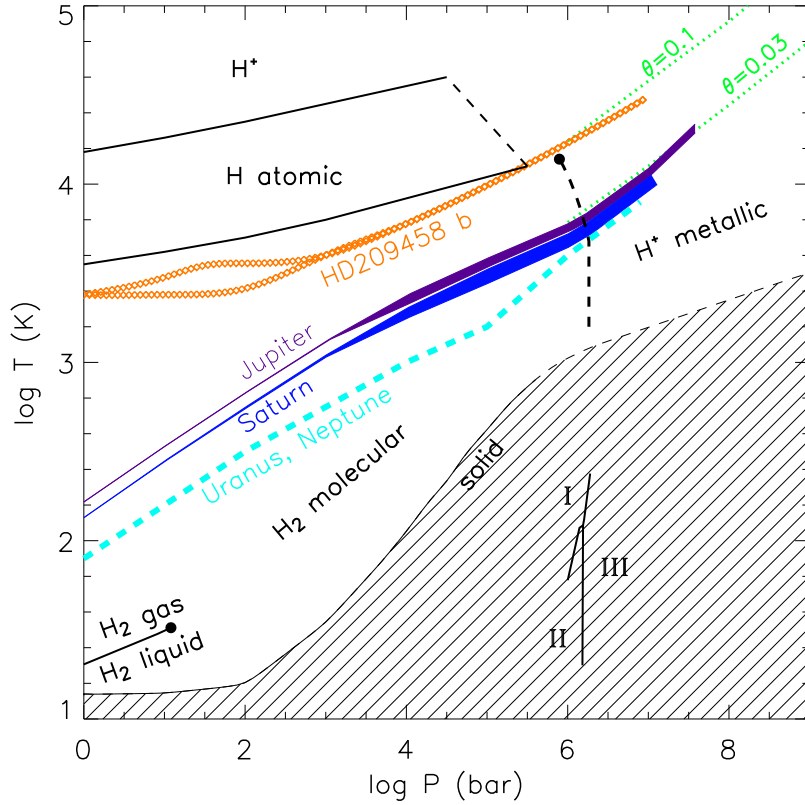
Figure 5: Phase diagram for hydrogen with the main phase transitions occurring in the fluid or gas phase. The temperature-pressure profiles for Jupiter, Saturn, Uranus, Neptune, and the exoplanet HD 209458 b are shown. The dashed nearly vertical line near 1 Mbar is indicative of the molecular to metallic transition (here it represents the so-called plasma phase transition as calculated by Saumon et al. (1995)). The region in which hydrogen is in solid phase (Datchi et al., 2000; Gregoryanz et al., 2003) is represented as a hatched area. The three phases (I,II,III) of solid hydrogen are shown (see Mao and Hemley, 1994). Values of the degeneracy parameter θ are indicated as dotted lines to the upper right corner of the figure.

suggested in Fig. 5 — or first metallizes in the molecular state H$_2$ remains to be clarified).

Recent laboratory measurements on fluid deuterium have been able to reach pressures above $\gtrsim 1$ Mbar, and provide new data in a region where the EOS remains most uncertain. Gas-guns experiments have been able to measure the reshock temperature (Holmes et al., 1995), near $T \sim$ 5000 K, $P \sim 0.8$ Mbar, and a rise in the conductivity of molecular hydrogen up to $T \sim 3000$ K, $P \sim 1.4$ Mbar, a sign that metallicity may have been reached (Weir et al., 1996). The following few years have seen the development of laser-induced shock compression (da Silva et al., 1997; Collins et al., 1998), pulsed-power shock compression (Knudson et al., 2004), and convergent shock wave experiments (Belov et al., 2002; Boriskov et al., 2005) in a high-pressure ($P = 0.3 - 4$ Mbar) high-temperature ($T \sim 6000 - 10^5$ K) regime. Unfortunately, experimental results along the principal Hugoniot of deuterium do not agree in this pressure range. Laser compression data give a maximum compression of ~ 6 while both the pulsed-power compression experiments and the convergent shock wave experiments find a value of ~ 4. Models that are partly calibrated with experimental data (Saumon et al., 1995; Ross, 1998; Ross and Yang, 2001) obtain a generally good agreement with the laser-compression data. However, the fact that independant models based on first principles (Militzer et al., 2001; Desjarlais, 2003; Bonev et al., 2004) yield low compressions strongly favors this solution.

The question of the existence of a first-order molecular to metallic transition of hydrogen (i.e. both molecular dissociation and ionisation occur simultaneously and discontinuously at the so-called plasma phase transition, or PPT) remains however. The critical line shown in fig. 5 corresponds to calculations by Saumon et al. (1995), but may be caused by artefacts in the free energy calculation. Recent Density Functional Theory (DFT) simulations by Bonev et al. (2004) indicate the possibility of a first order liquid-liquid transition but other path-integral calculations (Militzer et al., 2001) do not. It is crucial to assess the existence of such a PPT because it would affect both convection and chemical composition in the giant planets.

A clear result from fig. 5 at least is that, as first shown by Hubbard (1968), the interiors of the hydrogen-helium giant planets are *fluid*, whatever their age: of course, they avoid the critical point for the liquid gas transition in hydrogen and helium, at very low temperatures, but they also lie comfortably above the solidification lines for hydrogen and helium. (An *isolated* Jupiter should begin partial solidification only after at least $\sim 10^3$ Ga of evolution.) They are considered to be fluid because at the high pressures and relatively modest temperatures in their interiors, coulomb interactions between ions play an important role in the EOS and yield a behavior that is more reminiscent of that of a liquid than that of a gas, contrary to what is the case in e.g. solar-like stars. For Uranus and Neptune, the situation is actually more complex because at large pressures they are not expected to contain hydrogen, but numerical simulations show that ices in their interior should be fluid as well (Cavazzoni et al., 1999).

Models of the interiors of giant planets require thermodynamically consistent EOSs calculated over the entire domain of pressure and temperature spanned by the planets during their evolution. Elements other than hydrogen, most importantly helium, should be consistently included. Such a calculation is a daunting task, and the only recent attempt at such an astrophysical EOS for substellar objects is that by Saumon et al. (1995). Another set of EOSs reproducing either the high- or low-compression results was calculated by Saumon and Guillot (2004) specifically for the calculation of present-day models of Jupiter and Saturn.

These EOSs have so far included other elements (including helium), only in a very approximative way, i.e. with EOSs for helium and heavy elements that are based on interpolations between somewhat ideal regimes, using an additive volume law, and neglecting the possibility of existence of phase separations (see Hubbard et al., 2002; Guillot et al., 2004, for further discussions).

3.3 Heat transport

Giant planets possess hot interiors, implying that a relatively large amount of energy has to be transported from the deep regions of the planets to their surface. This can either be done by radiation, conduction, or, if these processes are not sufficient, by convection. Convection is generally ensured by the rapid rise of the opacity with increasing pressure and temperature. At pressures of a bar or more and relatively low temperatures (less than 1000 K), the three dominant sources of opacities are water, methane and collision-induced absorption by hydrogen molecules.

However, in the intermediate temperature range between ~ 1200 and 1500 K, the Rosseland opacity due to the hydrogen and helium absorption behaves differently: the absorption at any given wavelength increases with density, but because the temperature also rises, the photons are emitted at shorter wavelengths, where the monochromatic absorption is smaller. As a consequence, the opacity can decrease. This was shown by Guillot et al. (1994) to potentially lead to the presence of a deep radiative zone in the interiors of Jupiter, Saturn and Uranus.

This problem must however be reanalyzed in the light of recent observations and analyses of brown dwarfs. Their spectra show unexpectedly wide sodium and potassium absorption lines (see Burrows, Marley & Sharp 2000), in spectral regions where hydrogen, helium, water, methane and ammonia are relatively transparent. It thus appears that the added contribution of these elements (if they are indeed present) would wipe out any radiative region at these levels (Guillot et al., 2004).

At temperatures above $1500 \sim 2000$ K two important sources of opacity appear: (i) the rising number of electrons greatly enhances the absorption of H_2^- and H^-; (ii) TiO, a very strong absorber at visible wavelengths is freed by the vaporization of $CaTiO_3$. Again, the opacity rises rapidly which ensures a convective transport of the heat. Still deeper, conduction by free electrons becomes more efficient, but the densities are found not to be high enough for this process to be significant, except perhaps near the central core (see Hubbard, 1968; Stevenson and Salpeter, 1977b).

While our giant planets seem to possess globally convective interiors, strongly irradiated extrasolar planets must develop a radiative zone just beneath the levels where most of the stellar irradiation is absorbed. Depending on the irradiation and characteristics of the planet, this zone may extend down to kbar levels, the deeper levels being convective. In this case, a careful determination of the opacities is necessary (but generally not possible) as these control the cooling and contraction of the deeper interior (see Ferguson et al., 2005, for a discussion of opacities and tables for substellar atmospheres and interiors).

3.4 The contraction and cooling histories of giant planets

The interiors of giant planets is expected to evolve with time from a high entropy, high θ value, hot initial state to a low entropy, low θ, cold degenerate state. The essential physics behind can be derived from the well-known virial theorem and the energy conservation which link the planet's internal energy E_i, gravitational energy E_g and luminosity through:

$$\xi E_i + E_g = 0, \tag{8}$$

$$L = -\frac{\xi - 1}{\xi}\frac{dE_g}{dt}, \tag{9}$$

where $\xi = \int_0^M 3(P/\rho)dm / \int_0^M u\,dm \approx <3P/\rho u>$, the brackets indicating averaging, and u is the specific internal energy. For a diatomic perfect gas, $\xi = 3.2$; for fully-degenerate non-relativistic electrons, $\xi = 2$.

Thus, for a giant planet or brown dwarf beginning its life mostly as a perfect H_2 gas, two third of the energy gained by contraction is radiated away, one third being used to increase E_i. The internal energy being proportional to the temperature, the effect is to heat up the planet. This represents the slightly counter-intuitive but well known effect that a star or giant planet initially heats up while radiating a significant luminosity (e.g. Kippenhahn and Weigert, 1994).

Let us now move further in the evolution, when the contraction has proceeded to a point where the electrons have become degenerate. For simplicity, we will ignore coulomb interactions and exchange terms, and assume that the internal energy can be written as $E_i = E_{el} + E_{ion}$, and that furthermore $E_{el} \gg E_{ion}$ (θ is small). Because $\xi \approx 2$, we know that half of the gravitational potential energy is radiated away and half of it goes into internal energy. The problem is to decide how this energy is split into an electronic and an ionic part. The gravitational energy changes with some average value of the interior density as $E_g \propto 1/R \propto \rho^{1/3}$. The energy of the degenerate electrons is essentially the Fermi energy: $E_{el} \propto \rho^{2/3}$. Therefore, $\dot{E}_{el} \approx 2(E_{el}/E_g)\dot{E}_g$. Using the virial theorem, this yields:

$$\dot{E}_{el} \approx -\dot{E}_g \approx 2L \tag{10}$$

$$L \approx -\dot{E}_{ion} \propto -\dot{T}. \tag{11}$$

The gravitational energy lost is entirely absorbed by the degenerate electrons, and the observed luminosity is due to the thermal cooling of the ions.

Several simplifications limit the applicability of this result (that would be valid in the white dwarf regime). In particular, the coulomb and exchange terms in the EOS introduce negative contributions that cannot be neglected. However, the approach is useful to grasp how the evolution proceeds: in its very early stages, the planet is very compressible. It follows a standard Kelvin-Helmoltz contraction. When degeneracy sets in, the compressibility becomes much smaller ($\alpha T \sim 0.1$, where α is the coefficient of thermal expansion), and the planet gets its luminosity mostly from the thermal cooling of the ions. The luminosity can be written in terms of a modified Kelvin-Helmoltz formula:

$$L \approx \eta \frac{GM^2}{R\tau}, \tag{12}$$

where τ is the age, and η is a factor that hides most of the complex physics. In the approximation that coulomb and exchange terms can be neglected, $\eta \approx \theta/(\theta+1)$. The poor compressibility of giant planets in their mature evolution stages imply that $\eta \ll 1$ ($\eta \sim 0.03$ for Jupiter): the luminosity is not obtained from the entire gravitational potential, but from the much more limited reservoir constituted by the thermal internal energy. Equation 12 shows that to first order, $\log L \propto -\log \tau$: very little time is spent at high luminosity values. In other words, the problem is (in most cases) weakly sensitive to initial conditions. However, it is to be noticed that with progresses in our capabilities to detect very young objects, i.e. planets and brown dwarfs of only a few million years of age, the problem of the initial conditions does become important (Marley et al., 2006).

Figure 6 shows more generally how giant planets, but also brown dwarfs and small stars see their luminosities evolve as a function of time. The $1/\tau$ slope is globally conserved, with some variations for brown dwarfs during the transient epoch of deuterium burning, and of course for stars, when they begin burning efficiently their hydrogen and settle on the main sequence: in that case, the tendency of the star to contract under the action of gravity is exactly balanced by thermonuclear hydrogen fusion.
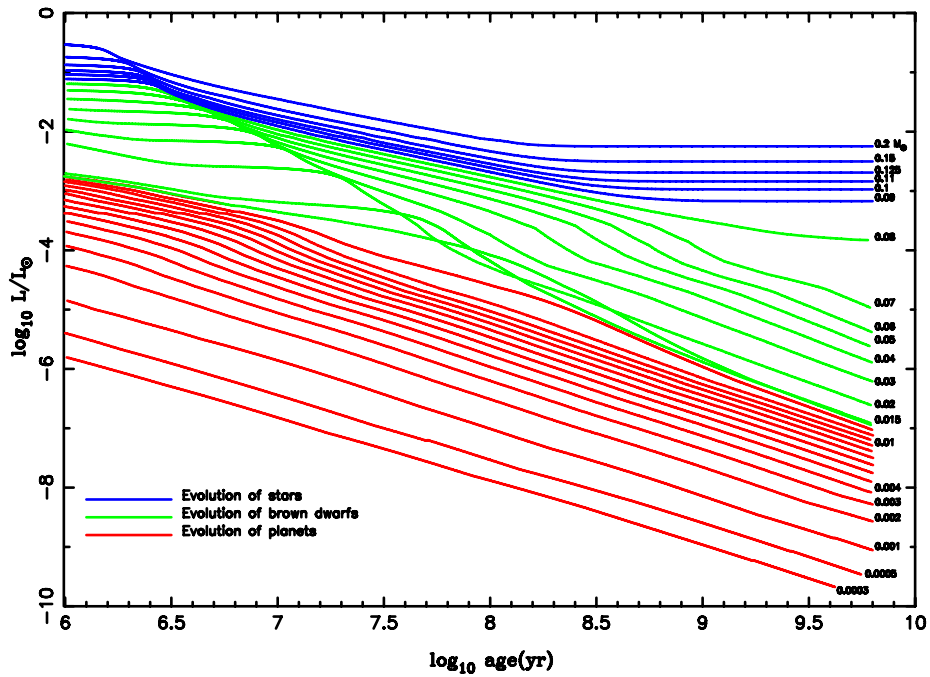
Figure 6: Evolution of the luminosity (in $L_\odot$) of solar-metallicity M dwarfs and substellar objects vs. time (in yr) after formation. In this figure, "brown dwarfs" are arbitrarily designated as those objects that burn deuterium, while those that do not are tentatively labelled "planets". Stars are objects massive enough to halt their contraction due to hydrogen fusion. Each curve is labelled by its corresponding mass in $M_\odot$, with the lowest three corresponding to the mass of Saturn, half the mass of Jupiter, and the mass of Jupiter. [From Burrows et al. (1997)].
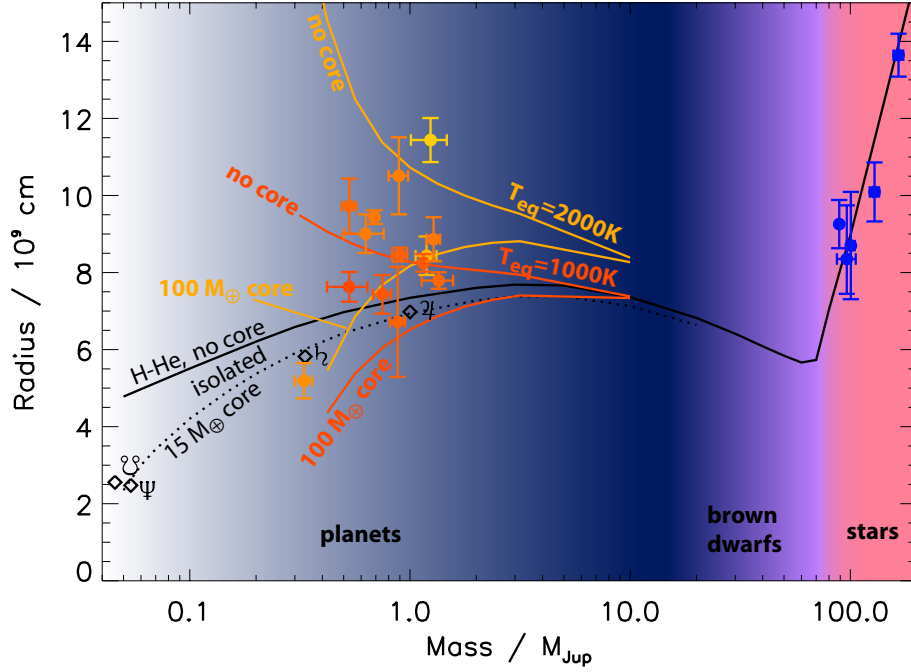
Figure 7: Theoretical and observed mass-radius relations. The black line is applicable to the evolution of solar composition planets, brown dwarfs and stars, when isolated or nearly isolated (as Jupiter, Saturn, Uranus and Neptune, defined by diamonds and their respective symbols), after 5 Ga of evolution. The dotted line shows the effect of a $15\,M_\oplus$ core on the mass-radius relation. Orange and yellow curves represent the mass-radius relations for heavily irradiated planets with equilibrium temperatures of 1000 and $2000\,$K, respectively, and assuming that 0.5% of the incoming stellar luminosity is dissipated at the center (see section 4.3). For each irradiation level, two cases are considered: a solar-composition planet with no core (top curve), and one with a $100\,M_\oplus$ central core (bottom curve). The transiting extrasolar giant planets for which a mass and a radius was measured are shown with points that are color-coded in function of the planet's equilibrium temperature. The masses and radii of very low mass stars are also indicated as blue points with error bars.

3.5 Mass-radius relation

The relation between mass and radius has very fundamental astrophysical applications. Most importantly it allows one to infer the gross composition of an object from a measurement of its mass and radius. This is especially relevant in the context of the discovery of extrasolar planets with both radial velocimetry and the transit method, as the two techniques yield relatively accurate determination of M and R.

Figure 7 shows mass-radius relations for compact degenerate objects from giant planets to brown dwarfs and low-mass stars. The right-hand side of the diagram shows a rapid increase of the radius with mass in the stellar regime which is directly due to the onset of stable thermonuclear reactions. In this regime, observations and theoretical models agree (see however Ribas, 2006, for a more detailed discussion). The left-hand side of the diagram is obviously more complex, and this can be understood by the fact that planets have much larger variations in compositions than stars, and because external factors such as the amount of irradiation they receive do affect their contraction in a significant manner.

Let us first concentrate on isolated or nearly-isolated gaseous planets. The black curves have a local maximum near $4\,\mathrm{M_J}$: at small masses, the compression is small so that the radius increases with mass. At large masses, degeneracy sets in and the radius decreases with mass.

This can be understood on the basis of polytropic models based on the assumption that $P = K\rho^{1+1/n}$, where K and n are constants. Because of degeneracy, a planet of large mass will tend to have $n \to 1.5$, while a planet a smaller mass will be less compressible ($n \to 0$). Indeed, it can be shown that in their inner 70 to 80% in radius isolated solar composition planets of 10, 1 and $0.1\,\mathrm{M_J}$ have $n = 1.3$, 1.0 and 0.6, respectively. From polytropic equations (e.g. Chandrasekhar, 1939):

$$R \propto K^{\frac{n}{3-n}} M^{\frac{1-n}{3-n}}. \tag{13}$$

Assuming that K is independant of mass, one gets $R \propto M^{0.16}$, M^0, and $M^{-0.18}$ for $M = 10$, 1 and $0.1\,\mathrm{M_J}$, respectively, in relatively good agreement with fig. 7 (the small discrepancies are due to the fact that the intrinsic luminosity and hence K depend on the mass considered).

Figure 7 shows already that the planets in our Solar System are not made of pure hydrogen and helium and require an additional fraction of heavy elements in their interior, either in the form of a core, or distributed in the envelope (dotted line).

For extrasolar planets, the situation is complicated by the fact that the intense irradiation that they receive plays a major role in their evolution. The present sample is already quite diverse, with equilibrium temperature (defined as the effective temperature corresponding to the stellar flux received by the planet) ranging from 1000 to 2500 K. Their composition is also quite variable, with some planets having large masses of heavy elements (Sato et al., 2005; Guillot et al., 2006). The orange and yellow curves in fig. 7 show theoretical results for equilibrium temperatures of 1000 and 2000 K, respectively. Two extreme models have been plotted: assuming a purely solar composition planet (top curve), and assuming the presence of a $100\,\mathrm{M_\oplus}$ central core (bottom curve). In each case, an additional energy source proportional to 0.5% of the incoming luminosity was also assumed (see discussion in § 4.3 hereafter).

The increase in radius for decreasing planetary mass for irradiated, solar-composition planets with little or no core can be understood using the polytropic relation (eq. 13), but accounting for variations of K as defined by the atmospheric boundary condition. Using the Eddington approximation, assuming $\kappa \propto P$ and a perfect gas relation in the atmosphere, one can show that $K \propto (M/R^2)^{-1/2n}$ and that therefore $R \propto M^{\frac{1/2-n}{2-n}}$. With $n = 1$, one finds $R \propto M^{-1/2}$. Strongly irradiated hydrogen-helium planets of small masses are hence expected to have the largest

radii which qualitatively explain the positions of the extrasolar planets in fig. 7. Note that this estimate implicitly assumes that n is constant throughout the planet. The real situation is more complex because of the growth of a deep radiative region in most irradiated planets, and because of structural changes between the degenerate interior and the perfect gas atmosphere.

In the case of the presence of a fixed mass of heavy elements, the trend is inverse because of the increase of mean molecular mass (or equivalently core/envelope mass) with decreasing total mass. Thus, small planets with a core are much more tightly bound and less subject to evaporation than those that have no core.

3.6   Rotation and the figures of planets

The mass and radius of a planet informs us on its global composition. Because planets are also rotating, one is allowed to obtain more information on their deep interior structure. The hydrostatic equation becomes more complex however:

$$\frac{\nabla P}{\rho} = \nabla \left(G \iiint \frac{\rho(\mathbf{r}')}{|\mathbf{r} - \mathbf{r}'|} d^3 \mathbf{r}' \right) - \boldsymbol{\Omega} \times (\boldsymbol{\Omega} \times \mathbf{r}), \tag{14}$$

where $\boldsymbol{\Omega}$ is the rotation vector. The resolution of eq. (14) is a complex problem. It can however be somewhat simplified by assuming that $|\boldsymbol{\Omega}| \equiv \omega$ is such that the centrifugal force can be derived from a potential. The hydrostatic equilibrium then writes $\nabla P = \rho \nabla U$, and the *figure* of the rotating planet is then defined by the $U = constant$ level surface.

One can show (e.g. Zharkov and Trubitsyn, 1978) that the hydrostatic equation of a fluid planet can then be written in terms of the mean radius $\overline{r}$ (the radius of a sphere containing the same volume as that enclosed by the considered equipotential surface):

$$\frac{1}{\rho}\frac{\partial P}{\partial \overline{r}} = -\frac{Gm}{\overline{r}^2} + \frac{2}{3}\omega^2 \overline{r} + \frac{GM}{\overline{R}^3}\overline{r}\varphi_\omega, \tag{15}$$

where M and $\overline{R}$ are the total mass and mean radius of the planet, and φ_ω is a slowly varying function of $\overline{r}$. (In the case of Jupiter, φ_ω varies from about 2×10^{-3} at the center to 4×10^{-3} at the surface.) Equations (5-7) remain the same with the hypothesis that the level surfaces for the pressure, temperature, and luminosity are equipotentials. The significance of rotation is measured by the ratio of the centrifugal acceleration to the gravity:

$$q = \frac{\omega^2 R_{\text{eq}}^3}{GM}. \tag{16}$$

As discussed in section 2.2, in some cases, the external gravity field of a planet can be accurately measured in the form of gravitational moments J_k (with zero odd moments for a planet in hydrostatic equilibrium) that measure the departure from spherical symmetry. Together with the mass, this provides a constraint on the interior density profile (see Zharkov and Trubitsyn (1974) -see also chapters by Van Hoolst and Sohl & Schubert):

$$
\begin{aligned}
M &= \iiint \rho(r, \theta) d^3 \tau, \\
J_{2i} &= -\frac{1}{MR_{\text{eq}}^{2i}} \iiint \rho(r, \theta) r^{2i} P_{2i}(\cos\theta) d^3 \tau,
\end{aligned}
$$

where $d\tau$ is a volume element and the integrals are performed over the entire volume of the planet.

Figure 8 shows how the different layers inside a planet contribute to the mass and the gravitational moments. The figure applies to Jupiter, but would remain relatively similar for other planets. Note however that in the case of Uranus and Neptune, the core is a sizable fraction of the total planet and contributes both to J_2 and J_4. Measured gravitational moments thus provide information on the external levels of a planet. It is only indirectly, through the constraints on the outer envelope that the presence of a central core can be infered. As a consequence, it is impossible to determine this core's state (liquid or solid), structure (differentiated, partially mixed with the envelope) and composition (rock, ice, helium...).
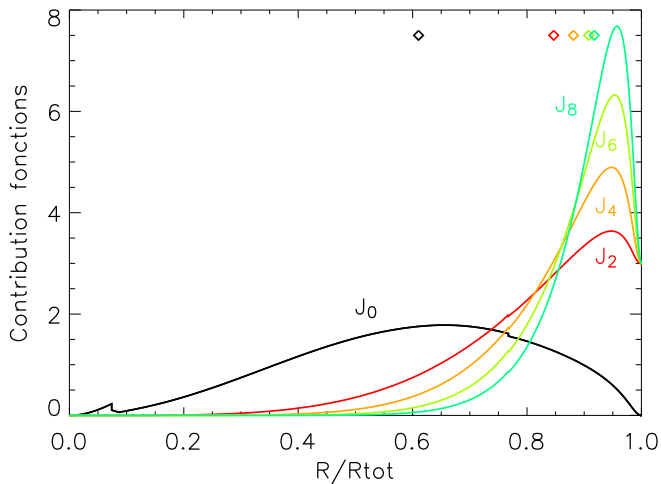

Figure 8: Contribution of the level radii to the gravitational moments of Jupiter. J_0 is equivalent to the planet's mass. The small discontinuities are caused by the following transitions, from left to right: core/envelope, helium rich/helium poor (metallic/molecular). Diamonds indicate the median radius for each moment.

For planets outside the solar system, although measuring their gravitational potential is utopic, their oblateness may be reachable with future space transit observations (Seager and Hui, 2002). Since the oblateness e is, to first order, proportionnal to q:

$$e = \frac{R_{eq}}{R_{eq} - R_{pol}} \approx \left(\frac{3}{2} \Lambda_2 + \frac{1}{2} \right) q \qquad (17)$$

(where $\Lambda_2 = J_2/q \approx 0.1$ to 0.2), it may be possible to obtain their rotation rate, or with a rotation measured from another method, a first constraint on their interior structure.

4 Interior structures and evolutions

4.1 Jupiter and Saturn

As illustrated by fig. 9, the simplest interior models of Jupiter and Saturn matching all observational constraints assume the presence of three main layers: (i) an outer hydrogen-helium envelope, whose
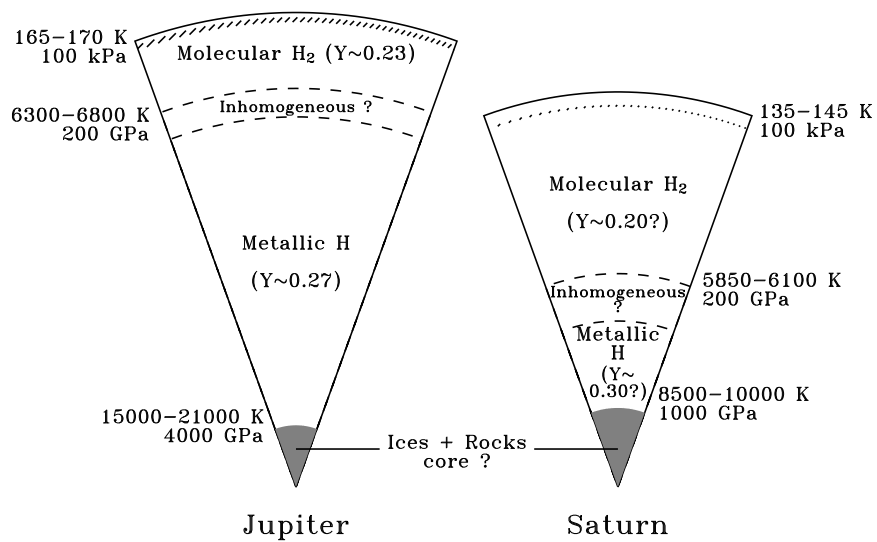
Figure 9: Schematic representation of the interiors of Jupiter and Saturn. The range of temperatures is estimated using homogeneous models and including a possible radiative zone indicated by the hashed regions. Helium mass mixing ratios Y are indicated. The size of the central rock and ice cores of Jupiter and Saturn is very uncertain (see text). In the case of Saturn, the inhomogeneous region may extend down all the way to the core which would imply the formation of a helium core. [Adapted from Guillot (1999b)].

global composition is that of the deep atmosphere; (ii) an inner hydrogen-helium envelope, enriched in helium because the whole planet has to fit the H/He protosolar value; (iii) a central dense core. Because the planets are believed to be mostly convective, these regions are expected to be globally homogeneous. (Many interesting thermochemical transformations take place in the deep atmosphere, but they are of little concern to us).

The transition from a helium-poor upper envelope to a helium-rich lower envelope is thought to take place through the formation of helium-rich droplets that fall deeper into the planet due to their larger density. These droplets form because of an assumed phase transition of helium in hydrogen at high pressures and low temperatures. Three-layer models implicitly make the hypothesis that this region is narrow. Indeed, calculations of such a phase separation in a fully-ionized plasma indicate a rapid decrease of the critical temperature with increasing pressure, with the consequence that helium would be unsoluble in a relatively small region in low-pressure metallic hydrogen. This region would progressively grow with time (e.g. Stevenson, 1982). However, DFT calculations have indicated that the critical temperature for helium demixing may rise with pressure (Pfaffenzeller et al., 1995), presumably in the regime where hydrogen is only partially ionized and bound states remain. This opens up the possibility that the inhomogeneous regions may be more extended, and that models more complex than the three-layer models may be needed, in particular in the case of Saturn (see below).

In the absence of these calculations, the three-layer models can be used as a useful guidance to a necessarily hypothetical ensemble of allowed structures and compositions of Jupiter and Saturn. These relatively extensive exploration of the parameter space have been performed by Saumon and Guillot (2004). The calculations assume that only helium is inhomogeneous in the envelope (the abundance of heavy elements is supposed to be uniform accross the molecular/metallic hydrogen transition). Many sources of uncertainties are taken into account however; among them, the most significant are on the equations of state of hydrogen and helium, the uncertain values of J_4 and J_6, the presence of differential rotation deep inside the planet, the location of the helium-poor to helium-rich region, and the uncertain helium to hydrogen protosolar ratio.

Their results indicate that Jupiter's core is smaller than $\sim 10\,\mathrm{M}_\oplus$, and that its global composition is pretty much unknown (between 10 to $42\,\mathrm{M}_\oplus$ of heavy elements in total). The models indicate that Jupiter is enriched compared to the solar value by a factor 1.5 to 8 times the solar value. This enrichment is compatible with a global uniform enrichment of all species near the atmospheric Galileo values, but include many other possibilities.

In the case of Saturn, the solutions depend less on the hydrogen EOS because the Mbar pressure region is comparatively smaller. The total amount of heavy elements present in the planet can therefore be estimated with a better accuracy than for Jupiter, and is between 20 and $30\,\mathrm{M}_\oplus$. In three-layer models with a discontinuity of the helium abundance at the molecular-metallic hydrogen interface but continuity of all other elements, the core masses found are between 10 and $22\,\mathrm{M}_\oplus$. However, because Saturn's metallic region is deeper into the planet, it mimics the effect that a central core would have on J_2. If we allow for variations in the abundance of heavy elements together with the helium discontinuity, then the core mass can become much smaller, and even solutions with no core can be found (Guillot 1999a). These solutions depend on the hypothetic phase separation of an abundant species (e.g. water), and generally cause an energy problem because of the release of considerable gravitational energy. However, another possibility is through the formation of an almost pure helium shell around the central core, which could lower the core masses by up to $7\,\mathrm{M}_\oplus$ (Fortney and Hubbard, 2003, Hubbard, personnal communication).

Concerning the *evolutions* of Jupiter and Saturn, the three main sources of uncertainty are, by order of importance: (1) the magnitude of the helium separation; (2) the EOS; (3) the at-

mospheric boundary conditions. Figure 10 shows an ensemble of possibilities that attempt to bracket the minimum and maximum cooling. In all cases, helium sedimentation is needed to explain Saturn's present luminosity (see Salpeter, 1973; Stevenson and Salpeter, 1977a; Hubbard, 1977). Recent models of Saturn's evolution appear to favor a scenario in which helium settles down almost to the central core (Hubbard et al., 1999; Fortney and Hubbard, 2003). In the case of Jupiter, the sedimentation of helium that appears to be necessary to explain the low atmospheric helium abundance poses a problem for evolution models because it appears to generally prolong its evolution beyond 4.55 Ga, the age of the Solar System. However, different solutions are possible, including improvements of the EOS and atmospheric boundary conditions, or even the possible progressive erosion of the central core that would yield a lower Jupiter's luminosity at a given age (Guillot et al., 2004).
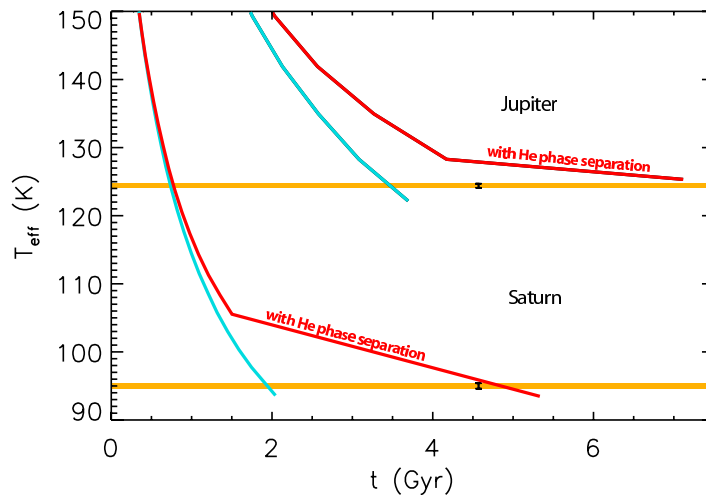

Figure 10: Final stages of evolution of Jupiter and Saturn. The present effective temperatures, reached after ~ 4.55 Ga of evolution, are indicated as horizontal orange lines. For each planet two models represent attempts to bracket the ensemble of possibilities, with the faster evolution corresponding to that of an homogeneous planet, while the slowest evolution includes the effect of helium settling in the last evolution phase. [Adapted from Hubbard et al. (1999) and Fortney and Hubbard (2003)].

4.2 Uranus and Neptune

Although the two planets are relatively similar, fig. 7 already shows that Neptune's larger mean density compared to Uranus has to be due to a slightly different composition: either more heavy elements compared to hydrogen and helium, or a larger rock/ice ratio. The gravitational moments impose that the density profiles lie close to that of "ices" (a mixture initially composed of e.g. H_2O, CH_4 and NH_3, but which rapidly becomes a ionic fluid of uncertain chemical composition in the planetary interior), except in the outermost layers, which have a density closer to that of hydrogen and helium (Marley et al., 1995; Podolak et al., 2000). As illustrated in fig. 11, three-layer models of Uranus and Neptune consisting of a central "rocks" core (magnesium-silicate and iron material), an ice layer and a hydrogen-helium gas envelope have been calculated (Podolak et al., 1991; Hubbard et al., 1995).
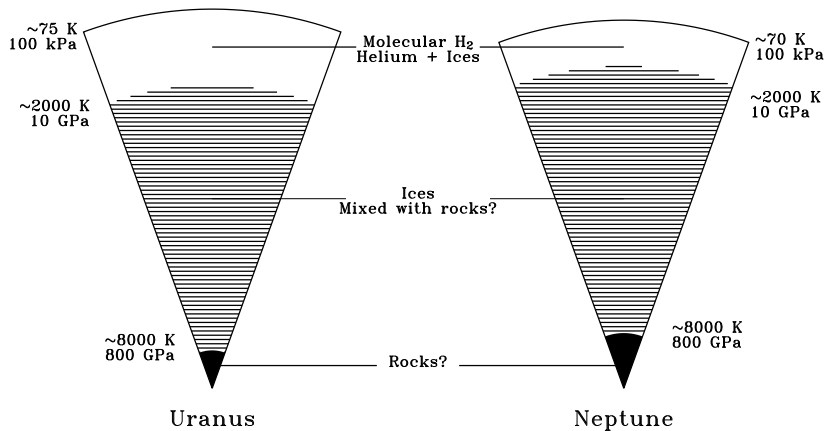
Figure 11: Schematic representation of the interiors of Uranus and Neptune. [Adapted from Guillot (1999b)].

The fact that models of Uranus assuming homogeneity of each layer and adiabatic temperature profiles fail in reproducing its gravitational moments seem to imply that substantial parts of the planetary interior are not homogeneously mixed (Podolak et al., 1995). This could explain the fact that Uranus' heat flux is so small: its heat would not be allowed to escape to space by convection, but through a much slower diffusive process in the regions of high molecular weight gradient. Such regions would also be present in Neptune, but much deeper, thus allowing more heat to be transported outward. The existence of these non-homogeneous, partially mixed regions are further confirmed by the fact that if hydrogen is supposed to be confined solely to the hydrogen-helium envelope, models predict ice/rock ratios of the order of 10 or more, much larger than the protosolar value of ~ 2.5. On the other hand, if we impose the constraint that the ice/rock ratio is protosolar, the overall composition of both Uranus and Neptune is, by mass, about 25% rock, $60 - 70\%$ ice, and $5 - 15\%$ hydrogen and helium (Podolak et al., 1991, 1995; Hubbard et al., 1995). Assuming both ice and rock are present in the envelope, an upper limit to the amount of hydrogen and helium present is $\sim 4.2\,\mathrm{M}_\oplus$ for Uranus and $\sim 3.2\,\mathrm{M}_\oplus$ for Neptune (Podolak et al., 2000). A lower limit of $\sim 0.5\,\mathrm{M}_\oplus$ for both planets can be inferred by assuming that hydrogen and helium are only present in the outer envelope at $P \lesssim 100\,\mathrm{kbar}$.

4.3   Irradiated giant planets

Although all extrasolar giant planets are in principle interesting, we focus here on the ones that orbit extremely close to their star because of the possibility to directly characterise them and measure their mass, radius and some properties of their atmosphere. Two planets are proxies for this new class of objects: the first extrasolar giant planet discovered, 51 Peg b, with an orbital period of $P = 4.23$ days, and the first *transiting* extrasolar giant planet, HD 209458 b, with $P = 3.52$ days. Both planets belong to the Pegasus constellation, and following astronomical conventions (e.g. Cepheids, named after δ Cephei), we choose to name giant planets orbiting close to their stars with periods shorter than 10 days "Pegasids" (alternatively, "hot Jupiters" is also found in the litterature).

With such a short orbital period, these planets are for most of them subject to an irradiation

from their central star that is so intense that the absorbed stellar energy flux can be about $\sim 10^4$ times larger than their intrinsic flux. The atmosphere is thus prevented from cooling, with the consequence that a radiative zone develops and governs the cooling and contraction of the interior (Guillot et al., 1996). Typically, for a planet like HD 209458 b, this radiative zone extends to kbar levels, $T \sim 4000\,\text{K}$, and is located in the outer 5% in radius (0.3% in mass) (Guillot and Showman, 2002).
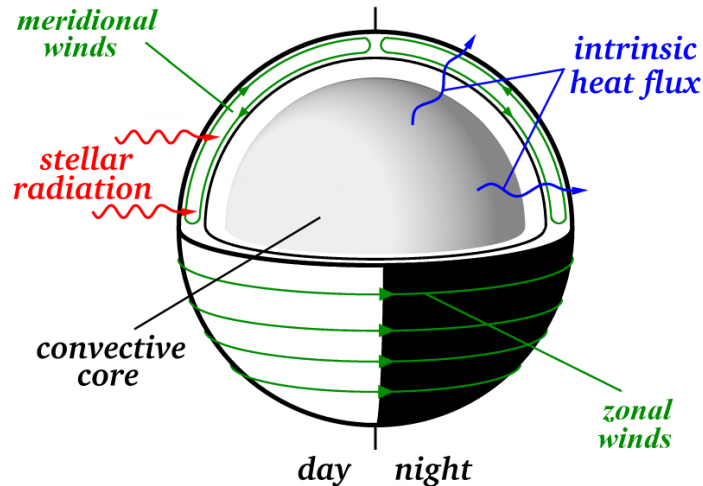

Figure 12: Conjectured dynamical structure of Pegasids (strongly irradiated extrasolar giant planets): At pressures larger than 100–800 bar, the intrinsic heat flux must be transported by convection. The convective core is at or near synchronous rotation with the star and has small latitudinal and longitudinal temperature variations. At lower pressures a radiative envelope is present. The top part of the atmosphere is penetrated by the stellar light on the day side. The spatial variation in insolation should drive winds that transport heat from the day side to the night side. [From Showman and Guillot (2002)].

Problems in the modeling of the evolution of Pegasids arise mostly because of the uncertain outer boundary condition. The intense stellar flux implies that the atmospheric temperature profile is extremely dependant upon the opacity sources considered. Depending on the chosen composition, the opacity data used, the assumed presence of clouds, the geometry considered, resulting temperatures in the deep atmosphere can differ by up to $\sim 600\,\text{K}$ (Seager and Sasselov, 2000; Goukenleuque et al., 2000; Barman et al., 2001; Sudarsky et al., 2003; Iro et al., 2005; Fortney et al., 2006). Furthermore, as illustrated by fig. 12, the strong irradiation and expected synchronisation of the planets implies that strong inhomogeneities should exist in the atmosphere with in particular strong ($\sim 500\,\text{K}$) day-night and equator-to-pole differences in effective temperatures (Showman and Guillot, 2002; Iro et al., 2005; Cooper and Showman, 2005; Barman et al., 2005), further complicating the modeling of the planetary evolution (see fig. fig. 13). Finally, another related problem is the presence of the radiative zone. Again, the composition is unknown and the opacity data are uncertain in this relatively high temperature ($T \sim 1500 - 3000\,\text{K}$) and high

pressure (up to ~ 1 kbar) regime.

We have seen in fig. fig. 7 that the measured masses and radii of transiting planets can be globally explained in the framework of an evolution model including the strong stellar irradiation and the presence of a variable mass of heavy elements, either in the form of a central core, or spread in the planet interior. However, when analyzing the situation for each planet, it appears that several planets are too large to be reproduced by standard models, i.e. models using the most up-to-date equations of state, opacities, atmospheric boundary conditions and assuming that the planetary luminosity governing its cooling is taken solely from the lost gravitational potential energy (see Section 3.1).

Figure 14 illustrates the situation for the particular case of HD209458b: unless using an unrealistically hot atmosphere, or arbitrarily increasing the internal opacity, or decreasing the helium content, one cannot reproduce the observed radius which is 10 to 20% larger than calculated (Bodenheimer et al., 2001, 2003; Guillot and Showman, 2002; Baraffe et al., 2003). The fact that the measured radius corresponds to a low-pressure ($\sim$mbar) level while the calculated radius corresponds to a level near 1 bar is not negligible (Burrows et al., 2003) but too small to account for the difference. This is problematic because while it is easy to invoke the presence of a massive core to explain the small size of a planet, a large size such as that of HD209458b requires an additional energy source, or significant modifications in the data/physics involved.

Bodenheimer et al. (2001) proposed that this large radius may be due to a small forced eccentricity ($e \sim 0.03$) of HD209458b, and subsequent tidal dissipation in the planet interior, but detailed observations indicate that the eccentricity is small, $e = 0.014 \pm 0.009$ (Laughlin et al., 2005), and observations of the secondary eclipse imply that this would further require a chance configuration of the orbit (Deming et al., 2005). Another proposed explanation also involving tidal dissipation of orbital energy is that the planet may be trapped in a Cassini state with a large orbital inclination (Winn and Holman, 2005), but it appears to have a low probability of occurrence (Levrard et al., 2006). Finally, a third possibility that would apply to *all* Pegasids is to invoke a downward transport of kinetic energy and its dissipation by tides (Showman and Guillot, 2002). This last possibility would require the various transiting planets to have different core masses to reproduce the observed radii (Guillot, 2005).

Recently, as more transiting Pegasids have been discovered, the number of anomalously large ones has increased to at least 3 for 11 planets, implying that this is not a rare event. This lends more weight to a mechanism that would apply to each planet. In this case, masses of heavy elements can be derived by imposing that all planets should be fitted by the same model with the same hypotheses. This can be done by inverting the results of fig. 7, as described by (Guillot et al., 2006). The method is applied to the known transiting Pegasids by the end of 2006 in fig. 15, a plot of the masses of heavy elements in the planets as a function of the metallicities of the parent star (which measures how rich a given star is in heavy elements compared to the Sun).

Figure 15 first shows that in some cases, large masses of heavy elements (up to $\sim 100\,\mathrm{M}_\oplus$ are necessary. This is in harmony with the composition inferred for HD149026b, i.e. around $70\,\mathrm{M}_\oplus$ of heavy elements, a conclusion that is hard to escape because of the low total mass and high irradiation of the planet (see Ikoma et al., 2006; Fortney et al., 2006). Furthermore, there seems to be a correlation between the mass of heavy elements inferred in the transiting planets, and the metallicity of the parent stars (Guillot et al., 2006), although this correlation has to be ascertained by more measurements. A caveat is important: these results are intrinsically model-dependent as they are based on the assumption that all planets receive an additionnal tidal heat flux that is proportionnal to the energy flux that they receive in the form of photons from the star. More transiting planets are needed to confirm or infirm this model, but the large variety in core masses,
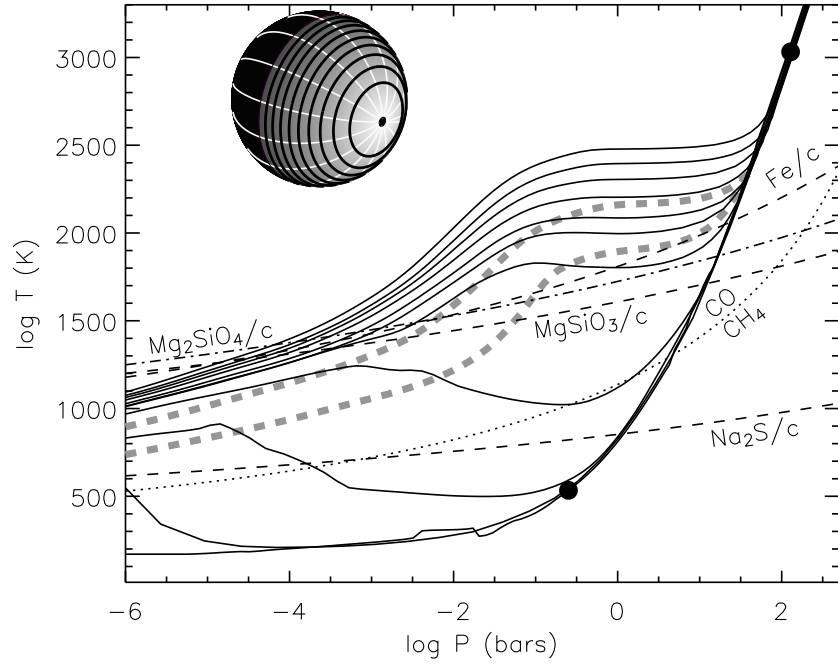
Figure 13: Temperature versus pressure for a sequence of locations in the atmosphere of HD209458b, assuming no horizontal redistribution of heat. Each sequence corresponds to a given direction of the incident flux relative to the surface normal. The approximate regions represented by the collection of T-P profiles are shown as solid black lines on the illustrative sphere. The topmost T-P profile corresponds to the sub-stellar point (black dot on the sphere). The terminator and night side (black hemisphere) are modeled with the non-irradiated profile (lowest T-P curve). The radiative-convective boundary at the sub-stellar point and on the night side are labeled with filled circles. The dashed lines indicate the approximate condensation curves for three common grain species. The dotted line indicates where gaseous CO and CH_4 concentrations are equal (CO is dominant to the left of this line). The thick, grey, dashed lines are T-P profiles calculated for a normal incident flux equal to 0.5 (top) and 0.25 (bottom) times that at the substellar point, as often used as approximate solutions for the day side, or entire atmosphere, respectively. [From Barman et al. (2005)].
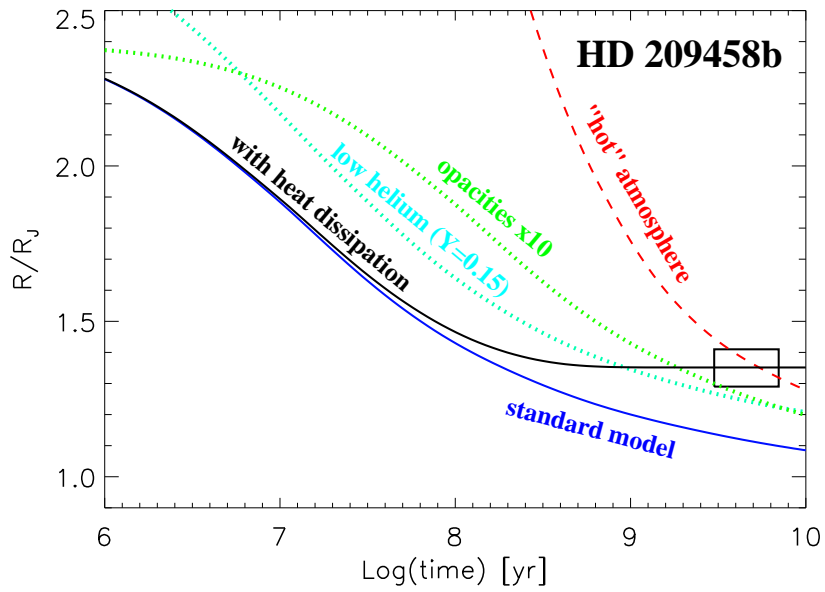
Figure 14: The contraction of HD209458b as a function of time can be compared to its measured radius and inferred age shown by the black box. Standard models (blue curve) for the evolution of that $0.69\,M_J$ planet generally yield a radius that is too small compared to the observations, even for a solar composition and no central core (a larger core and -in most cases- larger amounts of heavy elements in the planet imply an even smaller size for a given age). Unrealistically low helium abundances or high opacities models lead to evolution tracks that barely cross the observational box. A possiblity is that heat is dissipated into the deep interior by stellar tides, either related to a non-zero orbital eccentricity forced by an unseen companion, or because of a constant transfer of angular momentum from the heated atmosphere to the interior (black curve). Alternatively, the atmosphere may be hotter than predicted due to heating by strong zonal winds and shear instabilities (red curve).
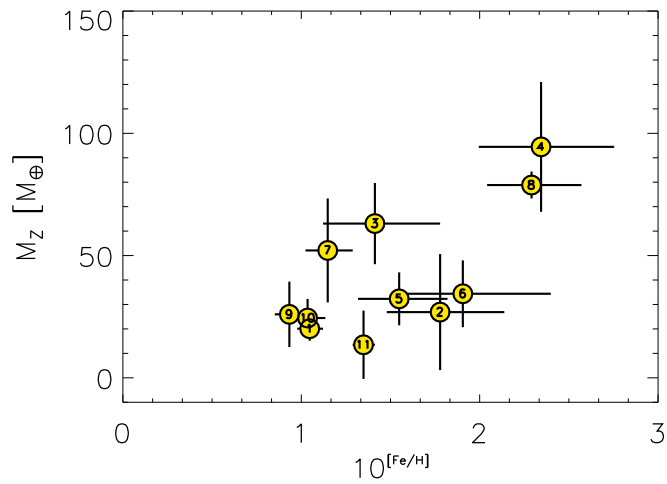
Figure 15: Mass of heavy elements in transiting Pegasids known by 2006 as a function of the metal content of the parent star relative to the Sun. The mass of heavy elements required to fit the measured radii is calculated on the basis of evolution models including an additional heat source slowing the cooling of the planet. This heat source is assumed equal to 0.5% of the incoming stellar heat flux (Showman and Guillot, 2002). Horizontal error bars correspond to the 1σ errors on the [Fe/H] determination. Vertical error bars are a consequence of the uncertainties on the measured planetary radii and ages. Note that the results, based on Guillot et al. (2006) are intrinsically model-dependent and may be affected by further discoveries of transiting planets.

and the absence of Pegasids around metal-poor stars ($[\text{Fe/H}] \lesssim -0.07$) as indicated by fig. 15 appear to be robust consequences of this work.

Another intriguing possibility concerning Pegasids is that of a sustained mass loss due to the high irradiation dose that the planets receive. Indeed, this effect was predicted (Burrows and Lunine, 1995; Guillot et al., 1996; Lammer et al., 2003) and detected (Vidal-Madjar et al., 2003, 2004), but its magnitude is still quite uncertain, by at least two orders of magnitude (Lammer et al., 2003; Lecavelier des Etangs et al., 2004; Yelle, 2006). The effect on the evolution is surprisingly limited, except at the final stages when an exponential mass loss appears in fully gaseous planets (Baraffe et al., 2004).

Finally, it is important to note that another class of planets awaits a direct characterisation by the transit method: that of ice or rock giants. Small-mass planets around $10\,\mathrm{M}_{\oplus}$ have been detected (e.g. Lovis et al., 2006; Beaulieu et al., 2006) but their radius is expected to be small (Guillot et al., 1996; Valencia et al., 2006), and we currently may not have the observational capability to test whether they transit in front of their star. This should be resolved by the space mission CoRoT (launched on 27 dec 2006) and Kepler (launch $\sim$ 2008). These objects are especially interesting but pose difficult problems in terms of structure because depending on their formation history, precise composition and location, they may be fluid, solid, or they may even possess a global liquid ocean (see Kuchner, 2003; Léger et al., 2004).

5 Implications for planetary formation models

The giant planets in our Solar System have in common possessing a large mass of hydrogen and helium, but they are obviously quite different in their aspect and in their internal structures. Although studies cannot be conducted with the same level of details, we can safely conclude that extrasolar planets show an even greater variety in composition and visible appearance.

A parallel study of the structures of our giant planets and of giant planets orbiting around other stars should provide us with key information regarding planet formation in the next decade or so. But, already, some conclusions, some of them robust, others still tentative, can be drawn (see also the chapter by Stevenson):

Giant planets formed in circumstellar disks, before these were completely dissipated:
This is a relatively obvious consequence of the fact that giant planets are mostly made of hydrogen and helium: these elements had to be acquired when they were still present in the disk. Because the observed lifetime of gaseous circumstellar disks is of the order of a few million years, this implies that these planets formed (i.e. acquired most of their final masses) in a few million years also, quite faster than terrestrial planets in the Solar System.

Giant planets migrated:
Although not cleanly demonstrated yet, there is evidence that the observed orbital distribution of extrasolar planets requires an inward migration of planets, and various mechanisms have been proposed for that (see Ida and Lin, 2004a; Alibert et al., 2005; Moorhead and Adams, 2005, ...etc.). Separately, it was shown that several properties of our Solar System can be explained if Jupiter, Saturn, Uranus and Neptune ended up the early formation phase in the presence of a disk with quasi-circular orbit, and with Saturn, Uranus and Neptune significantly closer to the Sun than they are now, and that these three planets subsequently migrated outward (Tsiganis et al., 2005).

Accretion played a key role for giant planet formation:
Several indications point towards a formation of giant planets that is dominated by accretion of heavy elements: First, Jupiter, Saturn, Uranus and Neptune are all significantly enriched in heavy elements compared to the Sun. This feature can be reproduced by core-accretion models,

for Jupiter and Saturn at least (Alibert et al., 2005). Second, the probability to find a giant planet around a solar-type star (with stellar type F, G or K) is a strongly rising function of stellar metallicity (Gonzalez, 1998; Santos et al., 2004; Fischer and Valenti, 2005), a property that is also well-reproduced by standard core accretion models (Ida and Lin, 2004b; Alibert et al., 2005). Third, the large masses of heavy elements inferred in some transiting extrasolar planets as well as the apparent correlation between mass of heavy elements in the planet and stellar metallicity (Guillot et al. (2006); see also Sato et al. (2005) and Ikoma et al. (2006)) is a strong indication that accretion was possible and that it was furthermore efficient. It is to be noted that none of these key properties are directly explained by formation models that assume a direct gravitational collapse (see Boss, 2004; Mayer et al., 2004).

Giant planets were enriched in heavy elements by core accretion, planetesimal delivery and/or formation in an enriched protoplanetary disk:
The giant planets in our Solar System are unambiguously enriched in heavy elements compared to the Sun, both globally, and when considering their atmosphere. This may also be the case of extrasolar planets, although the evidence is still tenuous. The accretion of a central core can explain part of the global enrichment, but not that of the atmosphere. The accretion of planetesimals may be a possible solution but in the case of Jupiter at least the rapid drop in accretion efficiency as the planet reaches appreciable masses ($\sim 100\,M_\oplus$ or so) implies that such an enrichment would have originally concerned only very deep layers, and would require a relatively efficient upper mixing of these elements, and possibly an erosion of the central core (Guillot et al., 2004).

Although not unambiguously explained, the fact that Jupiter is also enriched in noble gases compared to the Sun is a key observation to understand some of the processes occuring in the early Solar System. Indeed, noble gases are trapped into solids only at very low temperatures, and this tells us either that most of the solids that formed Jupiter were formed at very low temperature to be able to trap gases such as Argon, probably as clathrates (Gautier et al., 2001; Hersant et al., 2004), or that the planet formed in an enriched disk as it was being evaporated (Guillot and Hueso, 2006).

6 Future prospects

We have shown that the compositions and structures of giant planets remain very uncertain. This is an important problem when attempting to understand and constrain the formation of planets, and the origins of the Solar System. However, the parallel study of giant planets in our Solar System by space missions such as Galileo and Cassini, and of extrasolar planets by both ground based and space programs has led to rapid improvements in the field, with in particular a precise determination of the composition of Jupiter's troposphere, and constraints on the compositions of a dozen of extrasolar planets.

Improvements on our knowledge of the giant planets requires a variety of efforts. Fortunately, nearly all of these are addressed at least partially by adequate projects in the next few years. The efforts that are necessary thus include (but are not limited to):

- Obtain a better EOS of hydrogen, in particular near the molecular/metallic transition. This will be addessed by the construction of powerful lasers such as the NIF in the US and the MégaJoule laser in France, and by innovative experiments such as shocks on pre-compressed samples. One of the challenges is not only obtaining higher pressures, but mostly lower temperatures than currently possible with single shocks. The parallel improvement of computing facilities should allow more extended numerical experiments.

- Calculate hydrogen-helium and hydrogen-water phase diagrams. (Other phase diagrams are desirable too, but of lesser immediate importance). This should be possible with new numerical experiments.

- Have a better yardstick to measure solar and protosolar compositions. This may be addressed by the analysis of the Genesis mission samples, or may require another future mission.

- Improve the values of J_4 and J_6 for Saturn. This will be done as part of the Cassini-Huygens mission. This should lead to better constraints, and possibly a determination of whether the interior of Saturn rotates as a solid body.

- Detect new transiting extrasolar planets, and hopefully some that are further from their star. The space missions CoRoT (2006) and Kepler (2008) should provide the detection and characterization of many tens, possibly hundreds of giant planets.

- Model the formation and evolution of ice giants such as Uranus, Neptune, and similar planets around other stars, in order to analyze detections of these objects and understand planetary formation.

- Improve the measurement of Jupiter's gravity field, and determine the abundance of water in the deep atmosphere. This will be done by the Juno mission (launch 2011) with a combination of an exquisite determination of the planet's gravity field and of radiometric measurements to probe the deep water abundance.

- It would be highly desirable to send a probe similar to the Galileo probe into Saturn's atmosphere. The comparison of the abundance of noble gases would discriminate between different models of the enrichment of the giant planets, and the additional measurement of key isotopic ratio would provide further tests to understand our origins.

Clearly, there is a lot of work on the road, but the prospects for a much improved knowledge of giant planets and their formation are bright.

References

Acuna, M. H., Connerney, J. E. P., Ness, N. F., 1983. The Z3 zonal harmonic model of Saturn's magnetic field Analyses and implications. *JGR* **88**, 8771–8778.

Alibert, Y., Mordasini, C., Benz, W., Winisdoerffer, C., 2005. Models of giant planet formation with migration and disc evolution. *A&A* **434**, 343–353.

Anderson, J. D., Campbell, J. K., Jacobson, R. A., Sweetnam, D. N., Taylor, A. H., 1987. Radio science with Voyager 2 at Uranus - Results on masses and densities of the planet and five principal satellites. *JGR* **92**, 14877–14883.

Atreya, S. K., Wong, M. H., Owen, T. C., Mahaffy, P. R., Niemann, H. B., de Pater, I., Drossart, P., Encrenaz, T., 1999. A comparison of the atmospheres of Jupiter and Saturn: deep atmospheric composition, cloud structure, vertical mixing, and origin. *Plan. Space Sci.* **47**, 1243–1262.

Bahcall, J. N., Pinsonneault, M. H., Wasserburg, G. J., 1995. Solar models with helium and heavy-element diffusion. *Reviews of Modern Physics* **67**, 781–808.

Baraffe, I., Chabrier, G., Barman, T. S., Allard, F., Hauschildt, P. H., 2003. Evolutionary models for cool brown dwarfs and extrasolar giant planets. The case of HD 209458. *A&A* **402**, 701–712.

Baraffe, I., Chabrier, G., Barman, T. S., Selsis, F., Allard, F., Hauschildt, P. H., 2005. Hot-Jupiters and hot-Neptunes: A common origin? *A&A* **436**, L47–L51.

Baraffe, I., Selsis, F., Chabrier, G., Barman, T. S., Allard, F., Hauschildt, P. H., Lammer, H., 2004. The effect of evaporation on the evolution of close-in giant planets. *A&A* **419**, L13–L16.

Barman, T. S., Hauschildt, P. H., Allard, F., 2001. Irradiated Planets. *ApJ* **556**, 885–895.

Barman, T. S., Hauschildt, P. H., Allard, F., 2005. Phase-Dependent Properties of Extrasolar Planet Atmospheres. *ApJ* **632**, 1132–1139.

Beaulieu, J.-P., Bennett, D. P., Fouqué, P., Williams, A., Dominik, M., Jorgensen, U. G., Kubas, D., Cassan, A., Coutures, C., Greenhill, J., Hill, K., Menzies, J., Sackett, P. D., Albrow, M., Brillant, S., Caldwell, J. A. R., Calitz, J. J., Cook, K. H., Corrales, E., Desort, M., Dieters, S., Dominis, D., Donatowicz, J., Hoffman, M., Kane, S., Marquette, J.-B., Martin, R., Meintjes, P., Pollard, K., Sahu, K., Vinter, C., Wambsganss, J., Woller, K., Horne, K., Steele, I., Bramich, D. M., Burgdorf, M., Snodgrass, C., Bode, M., Udalski, A., Szymański, M. K., Kubiak, M., Więckowski, T., Pietrzyński, G., Soszyński, I., Szewczyk, O., Wyrzykowski, Ł., Paczyński, B., Abe, F., Bond, I. A., Britton, T. R., Gilmore, A. C., Hearnshaw, J. B., Itow, Y., Kamiya, K., Kilmartin, P. M., Korpela, A. V., Masuda, K., Matsubara, Y., Motomura, M., Muraki, Y., Nakamura, S., Okada, C., Ohnishi, K., Rattenbury, N. J., Sako, T., Sato, S., Sasaki, M., Sekiguchi, T., Sullivan, D. J., Tristram, P. J., Yock, P. C. M., Yoshioka, T., 2006. Discovery of a cool planet of 5.5 Earth masses through gravitational microlensing. *Nature* **439**, 437–440.

Belov, S. I., Boriskov, G. V., Bykov, A. I., Il'Kaev, R. I., Luk'yanov, N. B., Matveev, A. Y., Mikhaǐlova, O. L., Selemir, V. D., Simakov, G. V., Trunin, R. F., Trusov, I. P., Urlin, V. D., Fortov, V. E., Shuǐkin, A. N., 2002. Shock Compression of Solid Deuterium. *Journal of Experimental and Theoretical Physics Letteres* **76**, 433–+.

Bézard, B., Lellouch, E., Strobel, D., Maillard, J.-P., Drossart, P., 2002. Carbon Monoxide on Jupiter: Evidence for Both Internal and External Sources. *Icarus* **159**, 95–111.

Bodenheimer, P., Laughlin, G., Lin, D. N. C., 2003. On the Radii of Extrasolar Giant Planets. *ApJ* **592**, 555–563.

Bodenheimer, P., Lin, D. N. C., Mardling, R. A., 2001. On the Tidal Inflation of Short-Period Extrasolar Planets. *ApJ* **548**, 466–472.

Bonev, S. A., Militzer, B., Galli, G., 2004. Ab initio simulations of dense liquid deuterium: Comparison with gas-gun shock-wave experiments. *Phys. Rev. B 69* (1), 014101–+.

Boriskov, G. V., Bykov, A. I., Il'Kaev, R. I., Selemir, V. D., Simakov, G. V., Trunin, R. F., Urlin, V. D., Shuikin, A. N., Nellis, W. J., 2005. Shock compression of liquid deuterium up to 109 GPa. *Phys. Rev. B 71* (9), 092104–+.

Borysow, A., Jorgensen, U. G., Zheng, C., 1997. Model atmospheres of cool, low-metallicity stars: the importance of collision-induced absorption. *A&A* **324**, 185–195.

Boss, A. P., 2004. Convective Cooling of Protoplanetary Disks and Rapid Giant Planet Formation. *ApJ* **610**, 456–463.

Briggs, F. H., Sackett, P. D., 1989. Radio observations of Saturn as a probe of its atmosphere and cloud structure. *Icarus* **80**, 77–103.

Burrows, A., Guillot, T., Hubbard, W. B., Marley, M. S., Saumon, D., Lunine, J. I., Sudarsky, D., 2000. On the Radii of Close-in Giant Planets. *ApJL* **534**, L97–L100.

Burrows, A., Lunine, J., 1995. Extrasolar Planets - Astronomical Questions of Origin and Survival. *Nature* **378**, 333–+.

Burrows, A., Marley, M., Hubbard, W. B., Lunine, J. I., Guillot, T., Saumon, D., Freedman, R., Sudarsky, D., Sharp, C., 1997. A Nongray Theory of Extrasolar Giant Planets and Brown Dwarfs. *ApJ* **491**, 856–+.

Burrows, A., Sudarsky, D., Hubbard, W. B., 2003. A Theory for the Radius of the Transiting Giant Planet HD 209458b. *ApJ* **594**, 545–551.

Busse, F. H., 1978. Magnetohydrodynamics of the Earth's Dynamo. *Annual Review of Fluid Mechanics* **10**, 435–462.

Campbell, J. K., Synnott, S. P., 1985. Gravity field of the Jovian system from Pioneer and Voyager tracking data. *AJ* **90**, 364–372.

Cavazzoni, C., Chiarotti, G. L., Scandolo, S., Tosatti, E., Bernasconi, M., Parrinello, M., 1999. Superionic and Metallic States of Water and Ammonia at Giant Planet Conditions. *Science* **283**, 44–+.

Cecconi, B., Zarka, P., 2005. Model of a variable radio period for Saturn. *Journal of Geophysical Research (Space Physics)* **110**, 12203–+.

Chandrasekhar, S., 1939. *An introduction to the study of stellar structure.* Chicago, Ill., The University of Chicago press [1939].

Charbonneau, D., Allen, L. E., Megeath, S. T., Torres, G., Alonso, R., Brown, T. M., Gilliland, R. L., Latham, D. W., Mandushev, G., O'Donovan, F. T., Sozzetti, A., 2005. Detection of Thermal Emission from an Extrasolar Planet. *ApJ* **626**, 523–529.

Charbonneau, D., Brown, T. M., Noyes, R. W., Gilliland, R. L., 2002. Detection of an Extrasolar Planet Atmosphere. *ApJ* **568**, 377–384.

Cohen, E. R., Taylor, B. N., 1987. The 1986 adjustment of the fundamental physical constants. *Reviews of Modern Physics* **59**, 1121–1148.

Collins, G. W., da Silva, L. B., Celliers, P., Gold, D. M., Foord, M. E., Wallace, R. J., Ng, A., Weber, S. V., Budil, K. S., Cauble, R., 1998. Measurements of the equation of state of deuterium at the fluid insulator-metal transition. *Science* **281**, 1178–1181.

Connerney, J. E. P., Ness, N. F., Acuna, M. H., 1982. Zonal harmonic model of Saturn's magnetic field from Voyager 1 and 2 observations. *Nature* **298**, 44–46.

Conrath, B. J., Gautier, D., 2000. Saturn Helium Abundance: A Reanalysis of Voyager Measurements. *Icarus* **144**, 124–134.

Cooper, C. S., Showman, A. P., 2005. Dynamic Meteorology at the Photosphere of HD 209458b. *ApJL* **629**, L45–L48.

da Silva, L. B., Celliers, P., Collins, G. W., Budil, K. S., Holmes, N. C., Barbee, T. W., Jr., Hammel, B. A., Kilkenny, J. D., Wallace, R. J., Ross, M., Cauble, R., Ng, A., Chiu, G., 1997. Absolute Equation of State Measurements on Shocked Liquid Deuterium up to 200 GPa (2 Mbar). *Physical Review Letters* **78**, 483–486.

Datchi, F., Loubeyre, P., Letoullec, R., 2000. Extended and accurate determination of the melting curves of argon, helium, ice (H2O), and hydrogen (H2). *Phys. Rev. B* **61**, 6535–6546.

Davies, M. E., Abalakin, V. K., Bursa, M., Lederle, T., Lieske, J. H., 1986. Report of the IAU/IAG/COSPAR working group on cartographic coordinates and rotational elements of the planets and satellites - 1985. *Celestial Mechanics* **39**, 103–113.

de Pater, I., Romani, P. N., Atreya, S. K., 1991. Possible microwave absorption by H2S gas in Uranus' and Neptune's atmospheres. *Icarus* **91**, 220–233.

Deming, D., Seager, S., Richardson, L. J., Harrington, J., 2005. Infrared radiation from an extrasolar planet. *Nature* **434**, 740–743.

Desjarlais, M. P., 2003. Density-functional calculations of the liquid deuterium Hugoniot, reshock, and reverberation timing. *Phys. Rev. B* **68** (6), 064204–+.

Fegley, B. J., Lodders, K., 1994. Chemical models of the deep atmospheres of Jupiter and Saturn. *Icarus* **110**, 117–154.

Ferguson, J. W., Alexander, D. R., Allard, F., Barman, T., Bodnarik, J. G., Hauschildt, P. H., Heffner-Wong, A., Tamanai, A., 2005. Low-Temperature Opacities. *ApJ* **623**, 585–596.

Fischer, D. A., Valenti, J., 2005. The Planet-Metallicity Correlation. *ApJ* **622**, 1102–1117.

Flasar, F. M., Achterberg, R. K., Conrath, B. J., Pearl, J. C., Bjoraker, G. L., Jennings, D. E., Romani, P. N., Simon-Miller, A. A., Kunde, V. G., Nixon, C. A., Bézard, B., Orton, G. S., Spilker, L. J., Spencer, J. R., Irwin, P. G. J., Teanby, N. A., Owen, T. C., Brasunas, J., Segura, M. E., Carlson, R. C., Mamoutkine, A., Gierasch, P. J., Schinder, P. J., Showalter, M. R., Ferrari, C., Barucci, A., Courtin, R., Coustenis, A., Fouchet, T., Gautier, D., Lellouch, E., Marten, A., Prangé, R., Strobel, D. F., Calcutt, S. B., Read, P. L., Taylor, F. W., Bowles, N., Samuelson, R. E., Abbas, M. M., Raulin, F., Ade, P., Edgington, S., Pilorz, S., Wallis, B., Wishnow, E. H., 2005. Temperatures, Winds, and Composition in the Saturnian System. *Science* **307**, 1247–1251.

Fortney, J. J., Hubbard, W. B., 2003. Phase separation in giant planets: inhomogeneous evolution of Saturn. *Icarus* **164**, 228–243.

Fortney, J. J., Saumon, D., Marley, M. S., Lodders, K., Freedman, R. S., 2006. Atmosphere, Interior, and Evolution of the Metal-rich Transiting Planet HD 149026b. *ApJ* **642**, 495–504.

Galopeau, P. H. M., Lecacheux, A., 2000. Variations of Saturn's radio rotation period measured at kilometer wavelengths. *JGR* **105**, 13089–13102.

Gautier, D., Conrath, B. J., Owen, T., De Pater, I., Atreya, S. K., 1995. *The Troposphere of Neptune*, pp. 547–611. Neptune and Triton, UofA Press.

Gautier, D., Hersant, F., Mousis, O., Lunine, J. I., 2001. Erratum: Enrichments in Volatiles in Jupiter: A New Interpretation of the Galileo Measurements. *ApJL* **559**, L183–L183.

Giampieri, G., Dougherty, M. K., Smith, E. J., Russell, C. T., 2006. A regular period for Saturn's magnetic field that may track its internal rotation. *Nature* **441**, 62–64.

Gierasch, P. J., Ingersoll, A. P., Banfield, D., Ewald, S. P., Helfenstein, P., Simon-Miller, A., Vasavada, A., Breneman, H. H., Senske, D. A., A4 Galileo Imaging Team, 2000. Observation of moist convection in Jupiter's atmosphere. *Nature* **403**, 628–630.

Gonzalez, G., 1998. Spectroscopic analyses of the parent stars of extrasolar planetary system candidates. *A&A* **334**, 221–238.

Goukenleuque, C., Bézard, B., Joguet, B., Lellouch, E., Freedman, R., 2000. A Radiative Equilibrium Model of 51 Peg b. *Icarus* **143**, 308–323.

Gregoryanz, E., Goncharov, A. F., Matsuishi, K., Mao, H.-K., Hemley, R. J., 2003. Raman Spectroscopy of Hot Dense Hydrogen. *Physical Review Letters 90* (17), 175701–+.

Guillot, T., 1999a. A comparison of the interiors of Jupiter and Saturn. *Plan. Space Sci.* **47**, 1183–1200.

Guillot, T., 1999b. Interior of Giant Planets Inside and Outside the Solar System. *Science* **286**, 72–77.

Guillot, T., 2005. THE INTERIORS OF GIANT PLANETS: Models and Outstanding Questions. *Annual Review of Earth and Planetary Sciences* **33**, 493–530.

Guillot, T., Burrows, A., Hubbard, W. B., Lunine, J. I., Saumon, D., 1996. Giant Planets at Small Orbital Distances. *ApJL* **459**, L35–L39.

Guillot, T., Hueso, R., 2006. The composition of Jupiter: sign of a (relatively) late formation in a chemically evolved protosolar disc. *MNRAS* **367**, L47–L51.

Guillot, T., Santos, N. C., Pont, F., Iro, N., Melo, C., Ribas, I., 2006. A correlation between the heavy element content of transiting extrasolar planets and the metallicity of their parent stars. *A&A* **453**, L21–L24.

Guillot, T., Showman, A. P., 2002. Evolution of "51 pegasus b-like" planets. *A&A* **385**, 156–165.

Guillot, T., Stevenson, D. J., Hubbard, W. B., Saumon, D., 2004. *The interior of Jupiter*, pp. 35–57. Jupiter. The Planet, Satellites and Magnetosphere.

Gulkis, S., Janssen, M. A., Olsen, E. T., 1978. Evidence for the depletion of ammonia in the Uranus atmosphere. *Icarus* **34**, 10–19.

Gurnett, D. A., Kurth, W. S., Hospodarsky, G. B., Persoon, A. M., Averkamp, T. F., Cecconi, B., Lecacheux, A., Zarka, P., Canu, P., Cornilleau-Wehrlin, N., Galopeau, P., Roux, A., Harvey, C., Louarn, P., Bostrom, R., Gustafsson, G., Wahlund, J.-E., Desch, M. D., Farrell, W. M., Kaiser, M. L., Goetz, K., Kellogg, P. J., Fischer, G., Ladreiter, H.-P., Rucker, H., Alleyne, H., Pedersen, A., 2005. Radio and Plasma Wave Observations at Saturn from Cassini's Approach and First Orbit. *Science* **307**, 1255–1259.

Hammel, H. B., de Pater, I., Gibbard, S. G., Lockwood, G. W., Rages, K., 2005. New cloud activity on Uranus in 2004: First detection of a southern feature at 2.2 μm. *Icarus* **175**, 284–288.

Harrington, J., Hansen, B. M., Luszcz, S. H., Seager, S., Deming, D., Menou, K., Cho, J. Y.-K., Richardson, L. J., 2006. The Phase-Dependent Infrared Brightness of the Extrasolar Planet υ Andromedae b. *Science* **314**, 623–626.

Hersant, F., Gautier, D., Lunine, J. I., 2004. Enrichment in volatiles in the giant planets of the Solar System. *Plan. Space Sci.* **52**, 623–641.

Holmes, N. C., Ross, M., Nellis, W. J., 1995. Temperature measurements and dissociation of shock-compressed liquid deuterium and hydrogen. *Phys. Rev. B* **52**, 15835–15845.

Hubbard, W. B., 1968. Thermal structure of Jupiter. *ApJ* **152**, 745–754.

Hubbard, W. B., 1977. The Jovian surface condition and cooling rate. *Icarus* **30**, 305–310.

Hubbard, W. B., 1989. *Structure and composition of giant planet interiors*, pp. 539–563. Origin and Evolution of Planetary and Satellite Atmospheres.

Hubbard, W. B., Burrows, A., Lunine, J. I., 2002. Theory of Giant Planets. *Ann. Rev. Astron. Astrophys.* **40**, 103–136.

Hubbard, W. B., Guillot, T., Marley, M. S., Burrows, A., Lunine, J. I., Saumon, D. S., 1999. Comparative evolution of Jupiter and Saturn. *Plan. Space Sci.* **47**, 1175–1182.

Hubbard, W. B., Pearl, J. C., Podolak, M., Stevenson, D. J., 1995. *The Interior of Neptune*, pp. 109–138. Neptune and Triton, UofA Press.

Hueso, R., Sánchez-Lavega, A., Guillot, T., 2002. A model for large-scale convective storms in Jupiter. *Journal of Geophysical Research (Planets)* **107**, 5–1.

Ida, S., Lin, D. N. C., 2004a. Toward a Deterministic Model of Planetary Formation. I. A Desert in the Mass and Semimajor Axis Distributions of Extrasolar Planets. *ApJ* **604**, 388–413.

Ida, S., Lin, D. N. C., 2004b. Toward a Deterministic Model of Planetary Formation. II. The Formation and Retention of Gas Giant Planets around Stars with a Range of Metallicities. *ApJ* **616**, 567–572.

Ikoma, M., Guillot, T., Genda, H., Tanigawa, T., Ida, S., 2006. On the Origin of HD 149026b. *ApJ* **650**, 1150–1159.

Ingersoll, A. P., Barnet, C. D., Beebe, R. F., Flasar, F. M., Hinson, D. P., Limaye, S. S., Sromovsky, L. A., Suomi, V. E., 1995. *Dynamic Meteorology of Neptune*, pp. 613–682. Neptune and Triton, UofA Press.

Iro, N., Bézard, B., Guillot, T., 2005. A time-dependent radiative model of HD 209458b. *A&A* **436**, 719–727.

Jacobson, R. A., Antreasian, P. G., Bordi, J. J., Criddle, K. E., Ionasescu, R., Jones, J. B., Mackenzie, R. A., Meek, M. C., Parcher, D., Pelletier, F. J., Owen, W. M., Jr., Roth, D. C., Roundhill, I. M., Stauch, J. R., 2006. The Gravity Field of the Saturnian System from Satellite Observations and Spacecraft Tracking Data. *AJ* **132**, 2520–2526.

Kippenhahn, R., Weigert, A., 1994. *Stellar Structure and Evolution*. Stellar Structure and Evolution, XVI, 468 pp. 192 figs.. Springer-Verlag Berlin Heidelberg New York. Also Astronomy and Astrophysics Library.

Knudson, M. D., Hanson, D. L., Bailey, J. E., Hall, C. A., Asay, J. R., Deeney, C., 2004. Principal Hugoniot, reverberating wave, and mechanical reshock measurements of liquid deuterium to 400 GPa using plate impact techniques. *Phys. Rev. B 69* (14), 144209–+.

Kuchner, M. J., 2003. Volatile-rich Earth-Mass Planets in the Habitable Zone. *ApJL* **596**, L105–L108.

Lammer, H., Selsis, F., Ribas, I., Guinan, E. F., Bauer, S. J., Weiss, W. W., 2003. Atmospheric Loss of Exoplanets Resulting from Stellar X-Ray and Extreme-Ultraviolet Heating. *ApJL* **598**, L121–L124.

Laughlin, G., Marcy, G. W., Vogt, S. S., Fischer, D. A., Butler, R. P., 2005. On the Eccentricity of HD 209458b. *ApJL* **629**, L121–L124.

Lecavelier des Etangs, A., Vidal-Madjar, A., McConnell, J. C., Hébrard, G., 2004. Atmospheric escape from hot Jupiters. *A&A* **418**, L1–L4.

Léger, A., Selsis, F., Sotin, C., Guillot, T., Despois, D., Mawet, D., Ollivier, M., Labèque, A., Valette, C., Brachet, F., Chazelas, B., Lammer, H., 2004. A new family of planets? "Ocean-Planets". *Icarus* **169**, 499–504.

Levrard, B., Morgado Correia, A., Chabrier, G., Baraffe, I., Selsis, F., Laskar, J., 2006. Tidal dissipation within hot Jupiters: a new appraisal. *ArXiv Astrophysics e-prints*.

Lindal, G. F., 1992a. The atmosphere of Neptune - an analysis of radio occultation data acquired with Voyager 2. *AJ* **103**, 967–982.

Lindal, G. F., 1992b. The atmosphere of Neptune - an analysis of radio occultation data acquired with Voyager 2. *AJ* **103**, 967–982.

Lindal, G. F., Sweetnam, D. N., Eshleman, V. R., 1985. The atmosphere of Saturn - an analysis of the Voyager radio occultation measurements. *AJ* **90**, 1136–1146.

Lindal, G. F., Wood, G. E., Levy, G. S., Anderson, J. D., Sweetnam, D. N., Hotz, H. B., Buckles, B. J., Holmes, D. P., Doms, P. E., Eshleman, V. R., Tyler, G. L., Croft, T. A., 1981. The atmosphere of Jupiter - an analysis of the Voyager radio occultation measurements. *JGR* **86**, 8721–8727.

Little, B., Anger, C. D., Ingersoll, A. P., Vasavada, A. R., Senske, D. A., Breneman, H. H., Borucki, W. J., The Galileo SSI Team, 1999. Galileo Images of Lightning on Jupiter. *Icarus* **142**, 306–323.

Lodders, K., Fegley, B., Jr., 1994. The origin of carbon monoxide in Neptunes's atmosphere. *Icarus* **112**, 368–375.

Lovis, C., Mayor, M., Pepe, F., Alibert, Y., Benz, W., Bouchy, F., Correia, A. C. M., Laskar, J., Mordasini, C., Queloz, D., Santos, N. C., Udry, S., Bertaux, J.-L., Sivan, J.-P., 2006. An extrasolar planetary system with three Neptune-mass planets. *Nature* **441**, 305–309.

Mao, H.-K., Hemley, R. J., 1994. Ultrahigh-pressure transitions in solid hydrogen. *Reviews of Modern Physics* **66**, 671–692.

Marley, M. S., Fortney, J. J., Hubickyj, O., Bodenheimer, P., Lissauer, J. J., 2006. On the Luminosity of Young Jupiters. *ArXiv Astrophysics e-prints*.

Marley, M. S., Gómez, P., Podolak, M., 1995. Monte Carlo interior models for Uranus and Neptune. *JGR* **100**, 23349–23354.

Marley, M. S., McKay, C. P., 1999. Thermal Structure of Uranus' Atmosphere. *Icarus* **138**, 268–286.

Mayer, L., Quinn, T., Wadsley, J., Stadel, J., 2004. The Evolution of Gravitationally Unstable Protoplanetary Disks: Fragmentation and Possible Giant Planet Formation. *ApJ* **609**, 1045–1064.

Mayor, M., Queloz, D., 1995. A Jupiter-Mass Companion to a Solar-Type Star. *Nature* **378**, 355–+.

Militzer, B., Ceperley, D. M., Kress, J. D., Johnson, J. D., Collins, L. A., Mazevet, S., 2001. Calculation of a Deuterium Double Shock Hugoniot from Ab Initio Simulations. *Physical Review Letters* **87** (26), A265502+.

Moorhead, A. V., Adams, F. C., 2005. Giant planet migration through the action of disk torques and planet planet scattering. *Icarus* **178**, 517–539.

Ness, N. F., Acuna, M. H., Behannon, K. W., Burlaga, L. F., Connerney, J. E. P., Lepping, R. P., 1986. Magnetic fields at Uranus. *Science* **233**, 85–89.

Ness, N. F., Acuna, M. H., Burlaga, L. F., Connerney, J. E. P., Lepping, R. P., 1989. Magnetic fields at Neptune. *Science* **246**, 1473–1478.

Owen, T., Mahaffy, P., Niemann, H. B., Atreya, S., Donahue, T., Bar-Nun, A., de Pater, I., 1999. A low-temperature origin for the planetesimals that formed Jupiter. *Nature* **402**, 269–270.

Pearl, J. C., Conrath, B. J., 1991. The albedo, effective temperature, and energy balance of Neptune, as determined from Voyager data. *JGR* **96**, 18921–+.

Pfaffenzeller, O., Hohl, D., Ballone, P., 1995. Miscibility of Hydrogen and Helium under Astrophysical Conditions. *Physical Review Letters* **74**, 2599–2602.

Podolak, M., Hubbard, W. B., Stevenson, D. J., 1991. *Model of Uranus' interior and magnetic field*, pp. 29–61. Uranus, UofA Press.

Podolak, M., Podolak, J. I., Marley, M. S., 2000. Further investigations of random models of Uranus and Neptune. *Plan. Space Sci.* **48**, 143–151.

Podolak, M., Weizman, A., Marley, M., 1995. Comparative models of Uranus and Neptune. *Plan. Space Sci.* **43**, 1517–1522.

Rages, K., Hammel, H. B., Lockwood, G. W., 2002. A Prominent Apparition of Neptune's South Polar Feature. *Icarus* **159**, 262–265.

Ribas, I., 2006. Masses and Radii of Low-Mass Stars: Theory Versus Observations. Ap&SS **304**, 89–92.

Ross, M., 1998. Linear-mixing model for shock-compressed liquid deuterium. *Phys. Rev. B* **58**, 669–677.

Ross, M., Yang, L. H., 2001. Effect of chainlike structures on shock-compressed liquid deuterium. *Phys. Rev. B 64* (13), 134210–+.

Roulston, M. S., Stevenson, D. J., 1995. Prediction of neon depletion in Jupiter's atmosphere. In: EOS, Volume 76, pp. 343.

Salpeter, E. E., 1973. On Convection and Gravitational Layering in Jupiter and in Stars of Low Mass. *ApJL* **181**, L83+.

Sanchez-Lavega, A., Lecacheux, J., Gomez, J. M., Colas, F., Laques, P., Noll, K., Gilmore, D., Miyazaki, I., Parker, D., 1996. Large-scale storms in Saturn's atmosphere during 1994. *Science* **271**, 631–634.

Santos, N. C., Israelian, G., Mayor, M., 2004. Spectroscopic [Fe/H] for 98 extra-solar planet-host stars. Exploring the probability of planet formation. *A&A* **415**, 1153–1166.

Sato, B., Fischer, D. A., Henry, G. W., Laughlin, G., Butler, R. P., Marcy, G. W., Vogt, S. S., Bodenheimer, P., Ida, S., Toyota, E., Wolf, A., Valenti, J. A., Boyd, L. J., Johnson, J. A., Wright, J. T., Ammons, M., Robinson, S., Strader, J., McCarthy, C., Tah, K. L., Minniti, D., 2005. The N2K Consortium. II. A Transiting Hot Saturn around HD 149026 with a Large Dense Core. *ApJ* **633**, 465–473.

Saumon, D., Chabrier, G., van Horn, H. M., 1995. An Equation of State for Low-Mass Stars and Giant Planets. *ApJS* **99**, 713–+.

Saumon, D., Guillot, T., 2004. Shock Compression of Deuterium and the Interiors of Jupiter and Saturn. *ApJ* **609**, 1170–1180.

Saumon, D., Hubbard, W. B., Burrows, A., Guillot, T., Lunine, J. I., Chabrier, G., 1996. A Theory of Extrasolar Giant Planets. *ApJ* **460**, 993–+.

Seager, S., Hui, L., 2002. Constraining the Rotation Rate of Transiting Extrasolar Planets by Oblateness Measurements. *ApJ* **574**, 1004–1010.

Seager, S., Sasselov, D. D., 2000. Theoretical Transmission Spectra during Extrasolar Giant Planet Transits. *ApJ* **537**, 916–921.

Seiff, A., Kirk, D. B., Knight, T. C. D., Young, R. E., Mihalov, J. D., Young, L. A., Milos, F. S., Schubert, G., Blanchard, R. C., Atkinson, D., 1998. Thermal structure of Jupiter's atmosphere near the edge of a 5-μm hot spot in the north equatorial belt. *JGR* **103**, 22857–22890.

Showman, A. P., Guillot, T., 2002. Atmospheric circulation and tides of "51 Pegasus b-like" planets. *A&A* **385**, 166–180.

Showman, A. P., Ingersoll, A. P., 1998. Interpretation of Galileo Probe Data and Implications for Jupiter's Dry Downdrafts. *Icarus* **132**, 205–220.

Simon-Miller, A. A., Gierasch, P. J., Beebe, R. F., Conrath, B., Flasar, F. M., Achterberg, R. K., the Cassini CIRS Team, 2002. New Observational Results Concerning Jupiter's Great Red Spot. *Icarus* **158**, 249–266.

Stevenson, D. J., 1982. Interiors of the giant planets. *Annual Review of Earth and Planetary Sciences* **10**, 257–295.

Stevenson, D. J., 1983. Planetary magnetic fields. *Reports of Progress in Physics* **46**, 555–557.

Stevenson, D. J., 1985. Cosmochemistry and structure of the giant planets and their satellites. *Icarus* **62**, 4–15.

Stevenson, D. J., Salpeter, E. E., 1977a. The dynamics and helium distribution in hydrogen-helium fluid planets. *ApJS* **35**, 239–261.

Stevenson, D. J., Salpeter, E. E., 1977b. The phase diagram and transport properties for hydrogen-helium fluid planets. *ApJS* **35**, 221–237.

Sudarsky, D., Burrows, A., Hubeny, I., 2003. Theoretical Spectra and Atmospheres of Extrasolar Giant Planets. *ApJ* **588**, 1121–1148.

Trafton, L. M., 1967. Model atmospheres of the major planets. *ApJ* **147**, 765–781.

Tsiganis, K., Gomes, R., Morbidelli, A., Levison, H. F., 2005. Origin of the orbital architecture of the giant planets of the Solar System. *Nature* **435**, 459–461.

Tyler, G. L., Sweetnam, D. N., Anderson, J. D., Borutzki, S. E., Campbell, J. K., Kursinski, E. R., Levy, G. S., Lindal, G. F., Lyons, J. R., Wood, G. E., 1989. Voyager radio science observations of Neptune and Triton. *Science* **246**, 1466–1473.

Valencia, D., O'Connell, R. J., Sasselov, D., 2006. Internal structure of massive terrestrial planets. *Icarus* **181**, 545–554.

Vidal-Madjar, A., Désert, J.-M., Lecavelier des Etangs, A., Hébrard, G., Ballester, G. E., Ehrenreich, D., Ferlet, R., McConnell, J. C., Mayor, M., Parkinson, C. D., 2004. Detection of Oxygen and Carbon in the Hydrodynamically Escaping Atmosphere of the Extrasolar Planet HD 209458b. *ApJL* **604**, L69–L72.

Vidal-Madjar, A., Lecavelier des Etangs, A., Désert, J.-M., Ballester, G. E., Ferlet, R., Hébrard, G., Mayor, M., 2003. An extended upper atmosphere around the extrasolar planet HD209458b. *Nature* **422**, 143–146.

von Zahn, U., Hunten, D. M., Lehmacher, G., 1998. Helium in Jupiter's atmosphere: Results from the Galileo probe helium interferometer experiment. *JGR* **103**, 22815–22830.

Warwick, J. W., Evans, D. R., Peltzer, G. R., Peltzer, R. G., Romig, J. H., Sawyer, C. B., Riddle, A. C., Schweitzer, A. E., Desch, M. D., Kaiser, M. L., 1989. Voyager planetary radio astronomy at Neptune. *Science* **246**, 1498–1501.

Warwick, J. W., Evans, D. R., Romig, J. H., Sawyer, C. B., Desch, M. D., Kaiser, M. L., Alexander, J. K., Gulkis, S., Poynter, R. L., 1986. Voyager 2 radio observations of Uranus. *Science* **233**, 102–106.

Weir, S. T., Mitchell, A. C., Nellis, W. J., 1996. Metallization of Fluid Molecular Hydrogen at 140 GPa (1.4 Mbar). *Physical Review Letters* **76**, 1860–1863.

Winn, J. N., Holman, M. J., 2005. Obliquity Tides on Hot Jupiters. *ApJL* **628**, L159–L162.

Wong, M. H., Mahaffy, P. R., Atreya, S. K., Niemann, H. B., Owen, T. C., 2004. Updated Galileo probe mass spectrometer measurements of carbon, oxygen, nitrogen, and sulfur on Jupiter. *Icarus* **171**, 153–170.

Yelle, R. V., 2006. Corrigendum to 'Aeronomy of extra-solar giant planets at small orbital distances' [Icarus 170 (2004) 167 179]. *Icarus* **183**, 508–508.

Zharkov, V. N., Trubitsyn, V. P., 1974. Internal constitution and the figures of the giant planets. *Physics of the Earth and Planetary Interiors* **8**, 105–107.

Zharkov, V. N., Trubitsyn, V. P., 1978. *Physics of planetary interiors.* Astronomy and Astrophysics Series, Tucson: Pachart, 1978.